MUD TRANSPORT IN TIDAL FLOW

by L.C. van Rijn

Content

MUD TRANSPORT IN TIDAL FLOW

by L.C. van Rijn

1. Introduction

This note is focused on the description of the local, time-dependent sediment transport over a muddy bed (mud fraction >70%) in tidal conditions including salinity effects.
The sediment transport equations are implemented in the quasi-steady mud transport model TMUD.xls and in the time-dependent model SUSTIM2DV, see Chapter 4.
Tide-induced and salinity-induced flow are briefly discussed in Chapters 2 and 3.

2. Tidal flow in prismatic and converging channels

An estuary is the (widened) outlet of a river to the sea and is governed by oscillating tidal flow coming from the (saline) sea and by the quasi-steady (fresh) water flow coming from the river in a complicated hydraulic system consisting of channels and shoals. The width and the area of the cross-section reduce in upstream (landward) direction with a river outlet at the end of the estuary resulting in a converging (funnel-shaped) channel system, see **Figure 2.1**. The bottom of the tide-dominated section is almost horizontal. Often, there is a mouth bar at the entrance of the estuary. Tidal flats or islands may be present along the estuary (deltas). The horizontal and vertical tide of this non-linear system can only be solved by a numerical model.

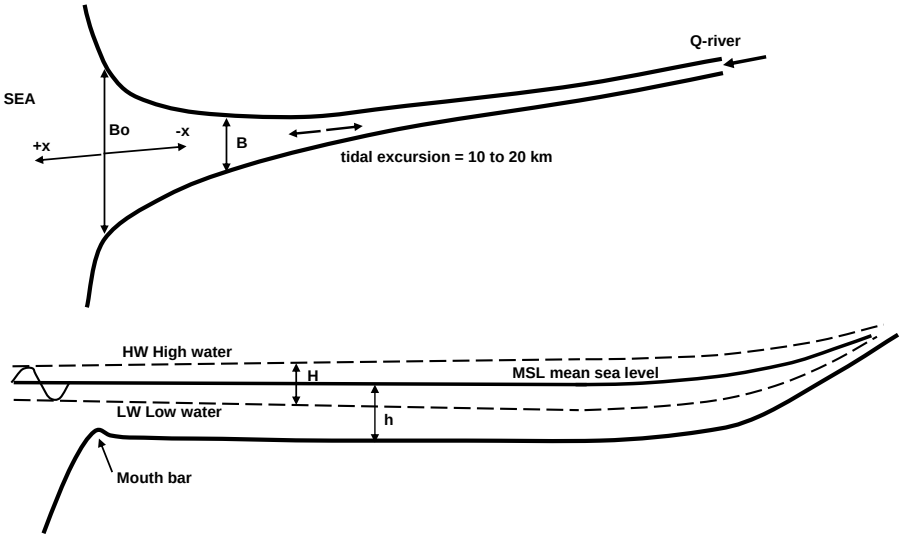

Figure 2.1 *Tidal estuary (plan shape and longitudinal section)*

The tidal range (H) in estuaries is affected by three dominant processes:

- shoaling or amplification due to the decrease of the width in landward direction,
- damping due to bottom friction,
- (partial reflection) at landward end of the estuary.

As a result of these processes there is a phase difference between the vertical (water levels) and horizontal (currents) tide. The horizontal tide has a phase lead of about 1 to 3 hours with respect to the vertical tide.
The variation of the tidal range H along the estuary can be, as follows:

- tidal range is constant $H = H_o$ (defined as an ***ideal*** estuary);
- tidal range increases $H > H_o$ (***amplified*** estuary);
- tidal range decreases $H < H_o$ (***damped*** estuary; weakly converging and prismatic channels).

with: H = tidal range and H_o = tidal range at entrance (mouth).

The offshore astronomical tide is composed of various constituents. The most important constituent is the semi-diurnal M_2-component. The first harmonic of this constituent is M_4. Generally, the M_4-component is small offshore, but rapidly increases within estuaries due to bottom friction and channel geometry. The M_2-component and its first harmonic M_4 dominate the non-linear processes within estuaries. Non-linear interaction between other constituents is also possible in shallow estuaries.
Analysis of field observations has shown that interaction of M_2 and its first harmonic M_4 explains the most important features of tidal asymmetries. The type of tidal distortion (flood or ebb dominance) depends on the relative phasing of M_4 to M_2.

The equations of mass and momentum for 1-dimensional depth-averaged flow in a converging tidal channel with a rectangular type of cross-section are given by:

$$\frac{b}{}\frac{\partial \eta}{\partial t} + \frac{\partial Q}{\partial x} = 0 \qquad (2.1)$$

$$\frac{1}{A}\frac{\partial Q}{\partial t} + \frac{g}{}\frac{\partial \eta}{\partial x} + \frac{Q\,|Q|}{C^2 A^2 R} = 0 \qquad (2.2)$$

in which: A = b h_o = cross-section area, b = width, h_o= depth to mean sea level, R = hydraulic radius and C = Chézy-coefficient are constants.

Basically, this set of non-linear equations can only be solved by a numerical model.
An analytical solution of the mass and momentum balance equations can also be obtained (Van Rijn, 2011) for a converging (funnel type) channel, if it is asumed that the:

- bottom is horizontal;
- channel depth to MSL is constant in space and time ($h = h_o+\eta$); depth h_o = constant;
- width $b = b_o e^{\beta x}$ with $\beta=1/L_b$= convergence coefficient, L_b = converging length scale, constant in time;
- convective acceleration ($\bar{u}\,\partial \bar{u}/\partial x = 0$) is neglected;
- friction is linear;
- fluid density is constant.

The solution reads as:

$$\eta = \hat{\eta}_o e^{(-0.5\beta+\mu)x} \cos(\omega t+kx) = \text{tidal water level} \qquad (2.3)$$

$$\bar{\bar{u}} = \hat{\bar{u}}_o e^{(-0.5\beta+\mu)x} \cos(\omega t+kx+\varphi) = \text{tidal velocity (cross-section averaged value)} \qquad (2.4)$$

$$\hat{\eta}_o = -h_o\,\hat{\bar{u}}_o\,(k/\omega)(1/\cos\varphi) = \text{peak tide amplitude at mouth x=0}$$

$$\hat{\bar{u}}_o = -(\hat{\eta}_o/h_o)(c)\cos\varphi = \text{peak tidal velocity at mouth} \qquad (2.5)$$

$$\tan\varphi = (0.5\beta+\mu)/k \qquad (2.6)$$

with x = negative in landward direction, k= wave number and μ= friction parameter, $c = \omega/k$ = wave speed, with $\beta=1/L_b$= convergence coefficient, β= 0 for prismatic channel, φ= phase shift between horizontal and vertical tide.

3. Salinity intrusion and salinity-induced flow in prismatic and converging tidal channels

3.1 Salinity intrusion

The most simple approach for determining the salinity distribution and the salt intrusion length in an estuary with river inflow is to use a cross-section-averaged and tide-averaged (1-dimensional) approach. This is most valid for ***well-mixed conditions*** (ρ is constant in vertical direction). Landward salt water intrusion in well-mixed conditions is caused by advective and dispersive processes. When the river discharge remains constant for some time (>> Tidal period), the salt penetration length will become constant on a tide-averaged time scale. The tide-averaged salt penetration length will decrease for increasing fresh water discharge and increase for decreasing discharge.
Figure 3.1 shows various types of cross-section averaged salt concentration distributions in a tidal estuary. The lower exponential distribution (– –) is a concave distribution (rounded inward) and mainly occurs in prismatic estuaries. The upper distribution (— . —) is a convex-type of distribution (rounded outward) and occurs in large estuaries with a small river at the landward side (Western Scheldt Estuary, The Netherlands; Thames Estuary, England).

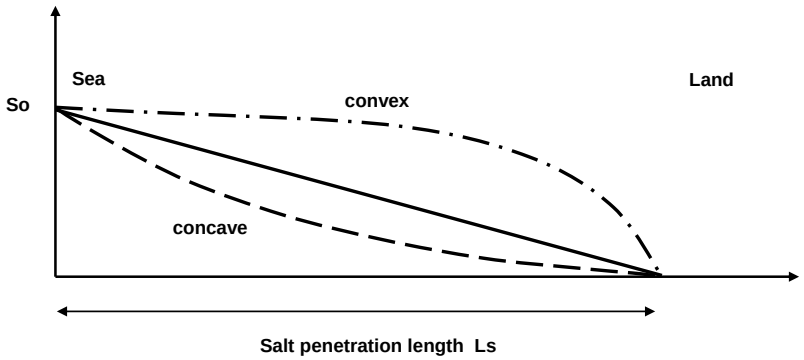

Figure 3.1 *Various types of salt concentration distributions in a tidal estuary*

Averaging the salt transport terms over the cross-section and over time yields the balance equation for advective seaward salt transport and dispersive landward salt transport in stationary conditions (constant river discharge for some days), as follows (Van Rijn 2011):

$$u_r \langle S \rangle - D \langle \partial S/\partial x \rangle = 0 \qquad (3.1)$$

with: u_r = cross-section averaged velocity based on river discharge (= Q/A; negative in seaward direction), S= cross-section averaged salt concentration (kg/m^3), D = dispersion coefficient, Q = river discharge (fresh water), A = b h = area of cross-section, b = average width of cross-section, h = h_o= average water depth to mean water level (assumed to be constant), <...> = time-averaged value (averaged over the tidal period T).

The salinity in an estuary channel can only be represented by the cross-section-averaged salinity if the lateral mixing proceeds relatively fast within the tidal cycle, which means that the channel width should be small compared to the channel length and width variations should be gradual.
The time-dependent salt balance equation can be formulated as (Van Rijn, 2011):

$$\partial S/\partial t + (u_{tide} - u_r)\, \partial S/\partial x - D_s \partial^2 S/\partial x^2 = 0 \qquad (3.2)$$

with: u_{tide}= tidal velocity (flood= positive; ebb= negative),u_r= fresh water velocity based on river discharge (negative in seaward direction).

The time-dependent solution can be described, as (Van Rijn, 2011):

$$S_{x,t}/S_o = [1 - \{x + x_b - (0.5L_e) + (0.5L_e)\cos(\omega t)\}/(x_b + L_{s,min})]^2 \qquad (3.3)$$

Assuming $x_b << L_{s,min}$, it follows that:

$$S_{x,t}/S_o = [1 - \alpha_x - 0.5\beta\,(1 - \cos(2\pi t/T)]^2 \qquad (3.4)$$

with: $\alpha_x = (x+x_b)/L_{s,min}$, $\beta = L_e/L_{s,min}$, x= location inside estuary from the mouth (x=0), L_e= tidal excursion = $U_{max}\,T/\pi$ and $L_{s,min}$= minimum tidal excursion at low water slack tide= $D_o/(0.5\,u_r)$, D_o= dispersion coefficient at mouth in the range of 500 to 1500 m^2/s and x_b= horizontal distance (positive value $x \cong 150\,h_o$) of the sea boundary seaward of the mouth (x= 0), T= tidal period.

If $\alpha_x - 0.5\beta\,(1 - \cos(2\pi t/T) \le 0$ then $S = S_o$.
If $\alpha_x - 0.5\beta\,(1 - \cos(2\pi t/T) \ge 1$ then $S = 0$.

The maximum salt intrusion length is: $L_{s,max} = L_{s,min} + L_e$
The fluid density is computed as: $\rho = \rho_{fresh} + 0.77\,S = 1000 + 0.77\,S$.

Equation(3.4) is implemented in the TMUD.xls model.

3.2 Residual flow velocity

Due to gravitational circulation a residual flow is generated in a tidal channel with fresh water inflow. The residual flow is landward near the bottom and seaward near the water surface.
Residual density-induced flow in a prismatic channel with tidal conditions can be determined by using the tide-averaged momentum equation. There are two main contributions: the free convection contribution arising from the density difference between salt water and fresh water and the fresh water discharge contribution.
Assuming well-mixed conditions and relatively small inertial terms (after averaging over the tidal cycle), the tide-averaged continuity and momentum equations for two-dimensional vertical flow in a prismatic channel with a rectangular cross-section (width>>depth) can be easily formulated (Van Rijn, 2011).

Assuming reasonably well-mixed conditions, the residual flow velocity profile can be expressed as:

$$U_{res,z} = M h_o^2\,[-(1/6)\,(z/h_o)^3 + (1/2)\,(z/h_o)^2 - (1/4)\,(z/h_o)] \qquad (3.5)$$
$$M = [g^{0.5}\,C]\,[\gamma\,(|U_{max}| + |\overline{u}_r|)\,h_o]^{-1}\,[(h_o/\rho)\,(\partial\rho/\partial x)]$$

with: z= level above bed (m), h= water depth at time t, h_o= tide-averaged water depth (m), U_{max}= peak tidal velocity (m/s), u_r= Q/(bh)= river velocity, $z_o = 0.033k_{s,c}$ = zero-velocity level, $k_{s,c}$ = current-related bed roughness (wave-current interaction is neglected), M=salinity factor ($m^{-1}s^{-1}$), C= Chézy-coefficient at time t, ρ_{sea}= density of sea water (kg/m^3), $\partial\rho/\partial x$= salinity-induced horizontal density gradient (input value; about 0.001 or 1 kg/m^3 per 1 km in stratified flow), ρ= depth-averaged and tide-averaged fluid density due to salinity= ρ_{fresh}+ 0.77 S (kg/m^3), ρ_{fresh} = fresh water density, S= salinity (0 to 25 kg/m^3), γ=coefficient (about 0.005 to 0.01).

The maximum residual velocity is approximately: $u_{res,max} = -0.035Mh_o^2$ about $z/h_o = 0.3$.

4. Mud transport in tidal flow

4.1 Mud transport in quasi-steady flow

The mud transport in quasi-steady flow depends on the upstream supply of mud (wash load) and the erodibility of the local muddy bed. In the case of a soft mud bed, the erosion of mud depends on the value excess bed-shear stress (bed-shear stress > critical bed-shear stress) and the mud characteristics. High mud concentrations (saturation suspension) almost uniformly distributed over the water depth may be generated in conditions with high velocities and bed-shear stresses, see also Section 4.3.
In the case of a firm mud bed with high resistance against erosion, the mud concentrations remain relatively small (<100 mg/l).

4.2 Mud transport in non-steady flow

4.2.1 Effect of time lags

In non-steady tidal flow, the actual sediment transport rate may be smaller (underload) or larger (overload) than the saturation (capacity) transport resulting in net erosion or deposition assuming sufficient availability of bed material (no armour layers).
The high near-bed concentrations can adjust rapidly to the new hydraulic conditions but the suspended load transport, however, needs time to adjust because the mud particles and flocs are carried upwards and downwards over the water depth.
Tidal flow is characterized by a daily ebb and flood cycle with a time scale of 6 to 12 hours (semidiurnal or diurnal tide) and by a neap-spring cycle with a time scale of about 14 days.
Sediment concentration measurements in tidal flow over a fine sediment bed show a continuous adjustment of the concentrations to the flow velocities with a lag period in the range of 0 to 60 minutes

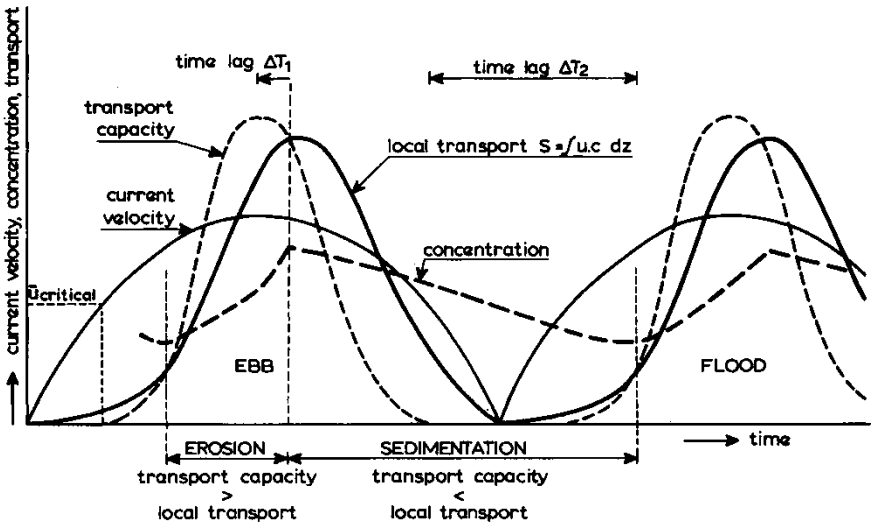

Figure 4.1 *Time lag of suspended sediment concentrations in tidal flow*

These basic transport processes in tidal flow are shown in **Figure 4.1**. Sediment particles go into suspension when the current velocity exceeds a critical value. In accelerating flow there always is a net vertical upward transport of sediment particles due to turbulence-related diffusive processes, which continues as long as the sediment transport capacity (saturation suspension) exceeds the actual transport rate. The time lag period ΔT_1 is the time period between the time of maximum flow and the time at which the transport capacity (saturation

suspension) is equal to the actual transport rate. After this latter time there is a net downward sediment transport because settling dominates yielding smaller concentrations and transport rates. In case of very fine sediments (silt and mud) or a large depth, the settling process can continue during the slack water period giving a large time lag (ΔT_2) which is defined as the period between the time of zero transport capacity and the start of a new erosion cycle. **Figure 4.1** shows that the suspended sediment transport during decelerating flow is always larger than during accelerating flow.

4.2.2 Effect of salinity stratification

In a stratified estuary a high-density salt wedge exists in the near-bed region resulting in relatively high near-bed densities and relatively low near-surface densities. The horizontal density-gradient generates a net tide-averaged landward flow near the bed and seaward flow near the surface. Stratified flow will result in damping of turbulence because turbulence energy is consumed in mixing of heavier fluid from a lower level to a higher level against the action of gravity.
The usual method to account for the salinity-related stratification effect on the velocity and concentration profiles is the reduction of the fluid mixing coefficient by introducing a damping factor related to the Richardson-number (Ri), as follows: $\varepsilon_f = \phi\, \varepsilon_{f,o}$ with $\varepsilon_{f,o}$=fluid mixing coefficient in fresh water, ϕ= F(Ri) = damping factor (< 1), Ri = local Richardson number.

4.3 Mud and fluid mud

4.3.1 Definitions

In most tidal basins the sediment bed consists of a mixture of sand and mud. The sand-mud mixture generally behaves as a mixture with cohesive properties when the mud fraction (all sediments<0.05 mm) is dominant (p_{mud}>0.3) and as a non-cohesive mixture when the sand fraction is dominant (p_{sand}>0.7). The distinction between non-cohesive mixtures and cohesive mixtures can be related to a critical mud content ($p_{mud,cr}$). Most important is the value of the clay/lutum-fraction (sediments<0.005 mm) in the mixture. Cohesive properties become dominant when the clay-fraction is larger than about 0.05 to 0.1. Assuming a clay-mud ratio of 0.5 to 0.25 for natural mud beds, the critical mud content will be about $p_{mud,cr}$= 0.2 to 0.4.

The term mud is commonly used to describe a mixture of fine-grained mineral sediments and organic material with cohesive properties. Field observations in tidal flow over a muddy bed show the presence of a cyclic process of erosion, transport, settling, deposition and consolidation.
Generally, a three-layer system can be distinguished in vertical direction (see **Figure 4.2**), as follows:

- **Consolidated mud layer** at the bottom with concentrations larger than about 300 kg/m³. The flocs and particles are supported by the internal floc framework. The mud interface is detectable by echosounding instruments (33 kHz).
- **Fluid mud suspension layer** with concentrations in the range of 10 to 300 kg/m³. The layer thickness is of the order of 0.1 to 1 m in normal conditions and up to 5 m in extreme conditions, as present at the Amazon shelf (Kineke and Sternberg, 1995). Marked interfaces (lutoclines) can be observed from echosounder recordings or from nuclear density recordings. The flocs and particles in the fluid mud layer are supported by fluid drag forces exerted by the escaping fluid (hindered settling effect). The fluid mud layer can be subdivided into a turbulent upper layer (mixed fluid mud; 10 to 100 kg/m³) and a laminar (viscous) lower layer (100 to 300 kg/m³), depending on conditions. The turbulent upper fluid mud layer will try to (i) mix mud from the laminar lower layer into the upper turbulent layer and (ii) mix fluid from the upper dilute suspension layer into the fluid mud layer if the upper fluid mud layer is more turbulent than the dilute suspension layer (in accelerating spring tide flow). This results in a decreasing

concentration in the upper fluid mud layer and a rise of the upper interface between the dilute layer and the fluid mud layer. If the dilute suspension layer is more turbulent than the fluid mud layer (in neap tide flow), the fluid mud layer will be relatively thin (much more stratified) and mud will be mixed up from the fluid mud layer into the dilute suspension layer by vortices from that layer. As fluid mud begins to form, the sediment concentration will because the fluid mud damps turbulence and impedes settling. Stratified fluid mud near the bed is enhanced by salinity stratification during neap tide (damping of turbulence) at the frontal zone between river water and sea water. These processes are well described by Kineke and Sternberg (1995) and Kineke et al. (1995) for the fluid mud system of the Amazon Shelf (South America). Transport of fluid mud will take place by tide-induced and wave-induced forces and gravity forces (sloping bottom).

The vertical structures of fluid mud can be subdivided into: a) mixed fluid mud, b) stratified fluid mud, and c) high-concentration fluid mud.
Mixed fluid mud exhibited vertically homogeneous concentration profiles with sediment concentration in the range 10 to 100 kg/m^3 (one lutocline at about 10 kg/m^3).
Stratified fluid mud is characterized by multiple lutoclines, with lutoclines at 10 kg/m^3 and at 100 kg/m^3; the elevation of the upper lutocline varies as a function of the acceleration of the tidal currents, while the lutocline of 100 kg/m^3 remains fairly stable. High-concentration fluid mud consists of a thin layer of very high sediment concentration, of the order of 100 to 300 kg/m^3, with relatively low sediment concentration (less than 1 kg/m^3) above it. The velocities within this type of fluid mud are very low.

- **Dilute mud suspension** with concentrations in the range of 0 to 10 kg/m^3, which are detectable by optical methods and mechanical sampling. Mud will be mixed into dilute suspension layer from the fluid mud layer if the the upper dilute layer is more turbulent than the fluid mud layer. Flocculation is dominant in the dilute suspension layer. The flocs and particles are supported by turbulence-induced fluid forces and transported by tide-driven and wind-driven currents.

Vertical layers of different densities are influenced by gravity processes which oppose the mixing processes. The stability of the system can be characterized by the gradient Richardson number (Ri) which includes the ratio of the concentration gradient and the velocity gradient. The concentration and velocity gradients are largest in the near-bed region. Larger mixing occurs for a larger velocity gradient. For Ri larger than about 0.2 (based on experimental data) with relatively large concentration gradients and relatively small velocity gradients, a stable system will be present (interfacial instabilities will die out and turbulence collapses).

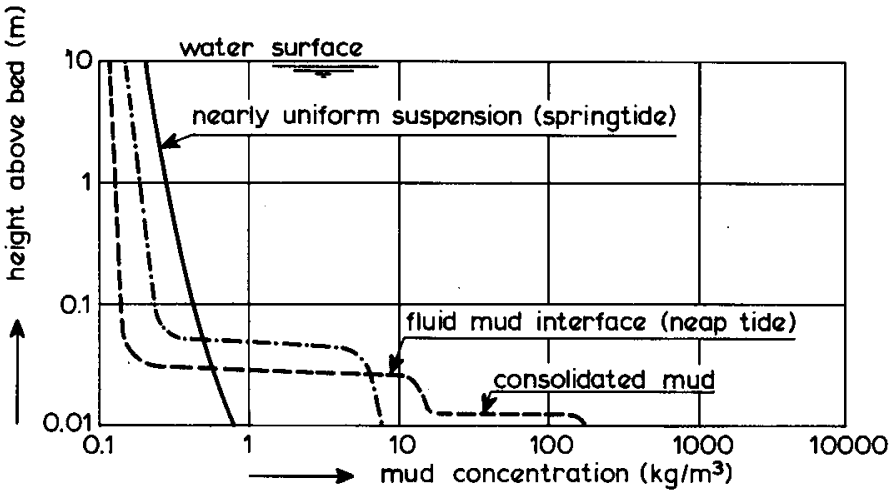

Figure 4.2 *Vertical distribution of mud concentrations*

Fluid mud can be defined as a high concentration aqueous suspension of fine-grained sediment in which settling is substantially hindered by the proximity of sediment grains and flocs, but which has not changed into an interconnected matrix of bonds strong enough to eliminate the potential for mobility (McAnally et al., 2007). When sediment flocs/aggregates are supported by the fluid, the water-sediment mixture behaves as a fluid with a viscosity on the order of 1000 times greater than the viscosity of water.
Fluid mud with a low organic content consists for a major part (50%) of clay-sized particles with sizes of 5 to 10 microns, with silt content usually secondary to clay.
Where fluid mud is persistent in relatively quiescent environments such as lakes, large amounts of organic matter can play a role in inhibiting dewatering and maintaining the fluid state of the bed
In comparison to the relatively quiescent, organic rich fluid muds found in some lakes, fluid muds in subaqueous deltas and estuaries and along high energy coasts tend to contain less organic matter (<5%). High organic matter and contaminant accumulation is more likely to be a problem in low energy fluid muds near population centers such as those commonly associated with siltation in harbor channels.

Fluid mud is often associated with a lutocline (a sudden change in sediment concentration with depth) and typically forms in near-bottom layers in lakes and estuaries, but can occur in any water body with sufficient fine-sediment supply and periods of low intensity flow.
Fluid mud typically exhibits concentrations of 10 to 100 kg/m^3 and wet bulk densities between 1050 and 1200 kg/m^3.
Fluid mud can flow down bottom slopes as a density current or horizontally as streaming under current or wave forcing.

Fluid mud in thin layers, as an intermediate stage in deposition (before the layer consolidates to form bed material) or bed erosion (by liquefaction before entrainment occurs) appears to be a common occurrence. Thicker layers, up to several meters deep, occur in many locations. In some ports and channels, fluid mud accumulates so rapidly that it exceeds the capacity of available dredges to keep the channel clear.

Fluid mud can be detected by echosounding using high-frequency and low-frequency signals. A high-frequency echosounder of 210 KHz reflects at the water-fluid interface, while a low-frequency echosounder of 33 KHz can penetrate into the mud layer and reflects at the more consolidated bed surface of about 1200 kg/m^3 (often used as nautical depth).

4.3.2 Saturation concentration

According to Winterwerp (2001), a saturation concentration exists for cohesive sediments in depositional conditions. When the velocities are decreasing after peak flow in tidal conditions, the sediments start to settle to form a layer of fluid mud, creating a two-layer fluid system. At the interface between the two layers, vertical turbulent mixing is damped strongly resulting in an overall decrease of the sediment-carrying capacity in the water column. At a certain moment the turbulence field collapses and the sediment concentrations are greatly reduced. The mud concentration just prior to this collapse is denoted by the term 'saturation concentration'. The conditions with concentrations larger and smaller than the saturation concentration are defined as supersaturation (overloading) and sub-saturation (underloading). Saturation concentration is proportional to $U^3/(hw_s)$ with U= depth-mean velocity, h= water depth and w_s= settling velocity and are in the range of 1 to 100 kg/m^3, depending on conditions.
The transport of very fine sediments in conditions with almost uniform suspensions (often defined as wash load) can described by an energy-based method as proposed by Bagnold (1962).
Bagnold (1962) derived the equilibrium or saturation sediment concentration (c_s) by considering the energy required to keep the sediment load in suspension and the energy dissipated by the transport of sediment.

The energy (per unit time and area) required to keep the suspended load in suspension is:

$$E_r = (\rho_s-\rho_w)\, g\, h\, (c_s/\rho_s)\, w_s \qquad (4.1)$$

with: c_s= equilibrium or saturation sediment concentration (mass); assumed to be uniform over depth, h=depth, w_s= effective fall velocity of suspended sediment.
The energy dissipated by the flow in transporting sediments is given by:

$$E_d = e_s\, (\tau_b\, u) \qquad (4.2)$$

with: e_s= efficiency coefficient (order of 0.025), $\tau_b = \rho_m g\, u^2/C^2$= bed-shear stress, u=depth-averaged velocity, C= Chézy-coefficient, $\rho_m = \rho_w(1+(s-1)c_s/\rho_s)$= mixture density.
Assuming $E_r = E_d$, yields the Bagnold-equation:

$$c_s = K\, \rho_s\, [(1+\alpha c_s)]\, [u^3/(g\, h\, w_s)] \qquad (4.3)$$

with: $K = [(e_s\, g)/((s-1)C^2)]$, $s=\rho_s/\rho_w$= relative density (2.65 for fresh water), $\alpha=(s-1)/\rho_s=0.00062$.
The K-value is of the order of 0.000015 for C=100 $m^{0.5}/s$.
Based on the concept of turbulence collapse in stratified flow, Winterwerp (2001) derived a similar expression for the saturation concentration with $K_w=0.7\, g^{1.5}/(s(s-1)C^3)$.
Expression (4.3) yields a dual sediment concentration and hence transport capacity if the hindered settling effect is included. Using $w_s = (1-c_s/c_{max})^5\, w_{s,o}$ for fine sediment, the relationship between the saturation concentration (c_s) and depth-averaged velocity (u) can be expressed, as:

$$u = [(\rho_s K)^{-1}\, (c_s)\, (1+\alpha c_s)^{-1}\, (1-c_s/c_{max})^5\, (g\, h\, w_{s,o})]^{0.3333} \qquad (4.4a)$$

or in dimensionless form:

$$u^3/(g\, h\, w_{s,o}) = [(\rho_s K)^{-1}\, (c_s)\, (1+\alpha c_s)^{-1}\, (1-c_s/c_{max})^5] \qquad (4.4b)$$

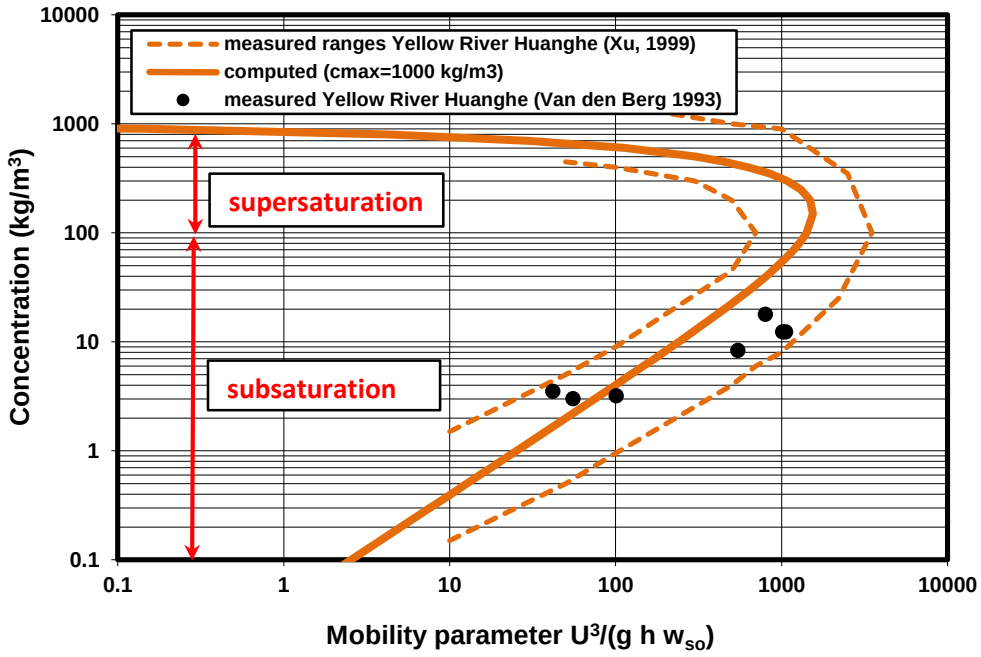

Figure 4.3 *Saturation concentration as function of dimensionless mobility parameter (h=10 m, C=100 $m^{0.5}/s$, c_{max}=1000 kg/m^3, $\nu=10^{-6}$ m^2/s)*

Equation (4.4b) yields a dual saturation concentration (c_s) for a given depth-averaged velocity, see **Figure 4.3**. The maximum sub-saturation concentration of the flow is about 150 kg/m^3 for particles in the range of 8 to 32 μm. Concentrations larger than about 150 kg/m^3 are defined as supersaturation or hyper-concentrations. These high hyper-concentrations and associated transport capacity strongly depend on the hindered settling process and on the upstream supply rate rather than on the local bed material. The lower values (sub-saturation range; minor hindered settling) can be transported by erosion of sediment from the local bed.
Saturation concentrations of clay (8 μm) in the range of 1 to 150 kg/m^3 can be transported at velocities of 1 to 2 m/s. The transport of silt particles (32 μm) at concentrations of 1 to 150 kg/m^3 requires larger velocities in the range of 4 to 5 m/s. Measured wash load concentration values and ranges for the Yellow River (Huanghe River) in China (Xu, 1999a,b; Van den Berg and Van Gelder, 1993) are also shown in Figure 4.3.2. Remarkably good agreement between computed and measured values can be observed using a maximum concentration of 1000 kg/m^3.
Similarly, thin layers of high-concentrations fluid mud (locally-generated) can be present in tidal estuaries, while thick fluid mud layers can be present in low areas and deeper channels due to supply from elsewhere.

Figure 4.3 shows measured sub-saturation depth-averaged concentrations of mud, silt and fine sand at various locations with tidal and river flow. The depth-averaged concentrations have been estimated from the available concentration profile data or from the ratio q_s/q with q_s= depth-integrated transport rate and q= water discharge rate. The basic data and conditions are given in **Table 4.1**. The mud concentrations are somewhat larger (factor 2 to 3) than the silt-fine sand concentrations. Mud concentrations in very large water depths are smaller than mud concentrations in smaller depths at the same depth-averaged velocity, because the bed-shear stresses are smaller for larger depths at the same flow velocity. Mud concentrations generated above a fluid mud bed are relatively large as the top layer of the fluid mud bed is eroded during tidal flow (over 0.1 to 0.5 m, Jiufa et al., 2001). Background mud concentrations for conditions with a sandy channel bed are also shown. The background mud concentrations, which are strongly supply-limited, are much smaller (factor 10) than the sub-satured mud concentrations over a muddy bed.

The sub-saturated concentrations (in mg/l) can be represented by the following equation (Bagnold-equation; see also Equation 4.3):

$$c_{mud} = \alpha_{mud}\, \rho_s\, 10^3\, u^3/(g\, w_s\, h) \qquad (4.5)$$

with:
c_{mud} = depth-averaged mud concentration (mg/l);
ρ_s = sediment density (kg/m^3);
u = depth-averaged flow velocity (m/s);
g = gravity acceleration (m/s^2);
w_s = settling velocity of mud (m/s);
h = water depth (m);
α_{mud} = coefficient ($\cong$ 0.000015).

Equation (4.5) is shown in **Figure 4.4** for two values of the water depth h= 5 m and h= 15 m. The mud settling velocity is assumed to be w_s= 0.0005 m/s (0.5 mm/s). Both curves are in the variation range for α_{mud} = 0.000015. A larger water depth yields smaller mud concentrations. Based on this, it can be concluded that saturated mud concentrations in tidal channels can be represented by the Bagnold equation (4.3, 4.5). This was also concluded by Winterwerp (2006).

Location	Water depth (m)	Bed conditions	Suspended sediment	Source
Nessmersiel mud Germany 1982-1987	0.5 to 1.5	fresh mud deposits < 200 kg/m^3	mud	Bauamt Kustenschutz, Norden 1987
Nessmersiel silt-mud Germany 1982-1987	0.5 to 1.5	sand-mud mixture > 500 kg/m^3	silt, fine sand and mud	Bauamt Kustenschutz, Norden 1987
Ems tidal river mud Germany June 1990	5 to 7	fluid mud (thin) 200-500 kg/m^3	mud	Winterwerp 2011
Ems tidal river mud Germany February 2006	5 to 7	fluid mud (thick) 200-500 kg/m^3	mud	Winterwerp 2011
Amazone tidal mouth Brasil 1990	15-20	fluid mud (thick) 200-500 kg/m^3	mud	Vinzon and Mehta 2003
Yangtze tidal estuary China September 1991	8-10	fluid mud (thick) 200-500 kg/m^3	mud	Jiufa et al., 2001
Elbe tidal river Germany 2002	13-15	sand-mud mixture > 500 kg/m^3	mud, silt and fine sand	BAW 2006/2007 Van Rijn 2016
Huanghe river China September 1987	5-10	sand-mud mixture > 500 kg/m^3	mud, silt and fine sand	Van den Berg and Van Gelder 1993
Ems tidal outer estuary Germany 2012	10-12	sand-mud mixture > 500 kg/m^3	mud, silt and fine sand	Van Maren et al. 2015
Elbe tidal outer estuary Germany 2002	10-15	sand-mud mixture > 500 kg/m^3	mud, silt and fine sand	BAW 2006/2007 Van Rijn 2016
Rotterdam tidal Water way Holland 2006	10-12	sand-mud mixture > 500 kg/m^3	sand-mud mixture	De Nijs 2012
Thames Estuary 2004	5-10 m	sand-mud mixture	mud	Baugh and Littlewood 2006

Table 4.1 *Basic data of measured mud, silt and fine sand concentrations*

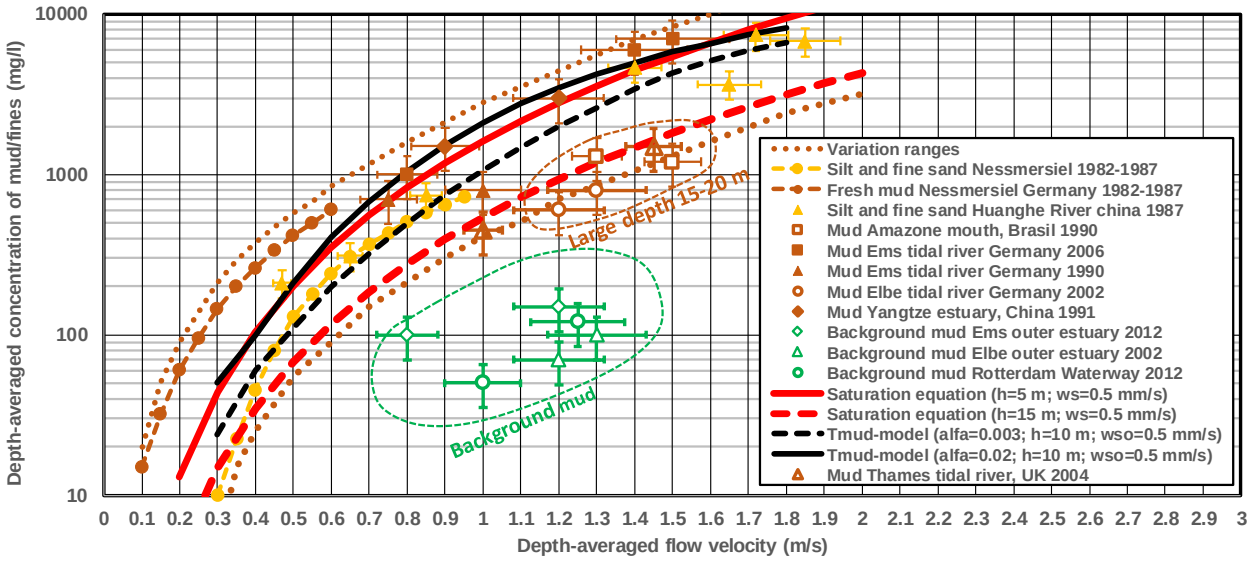

Figure 4.4 *Mud and silt concentrations as function of depth-averaged flow velocity*

4.3.3 Fluid mud formation

Fluid mud can form under various conditions:

Supply-dominated

- in quiescent environments where relatively large mud concentrations can settle and aggregate; in river, lake, estuarine and shelf environments when the amount of fine sediment entering the near-bed layer is greater than the dewatering rate;
- during decelerating tidal flow (especially during neap tides); during slack water a thin, temporary layer of fluid mud can be formed from the concentrations settling out from above (thickness of 0.01 to 0.1 m; concentration of 10 to 100 kg/m^3); when the water and mud move into deeper channels, the suspension becomes supersaturated due to the smaller bed-shear stresses and velocities in the channel (larger depth; smaller velocity); the vertical turbulence and concentration profiles collapse/decline, forming a thin (order of 0.1 m) fluid mud layer in the channel;
- gravity flows or density flows of a sediment-fluid mixture generated elsewhere moving downslope under the action of gravity into a deeper navigation channel or filling low areas; three types of gravity flows are distinguished: a) flows supported in suspension by the turbulence generated by their own down-slope movement; b) non-turbulent fluid mud gravity flows; and c) gravity flows supported by the shear associated with ambient currents and waves;
- fluid mud formations may be caused by open water dredged material disposal.

Locally-generated

- high concentrations generated at the muddy beds near the edge of the salt wedge (turbidity maximum) in highly stratified estuaries;
- fluidization by wave action; fluidization of a cohesive sediment bottom occurs when the soil matrix is destroyed by excess pore pressure buildup; the upwards pore water velocity exceeds the settling velocity of the grains; fluidization proceeds from the muddy bottom up, depending on the thickness of the muddy bottom and the degree of consolidation; sediment deposits (top layer of the bed) can be easily fluidized by wave action; when wave action stops, the fluid mud quickly reconsolidates into a fairly firm bed;
- fluid mud can be generated by vessel-induced agitation of soft mud beds.

Locally-generated fluid mud can easily form in tidal flow over a soft muddy bed. Sediment begins to settle during the decelerating stages of tidal cycles. As the flow continues to decrease towards slack, the lutoclines settle towards the bed, forming a thin layer of fluid mud. Dilute mud concentrations in tidal flow generally are in the range of 0.1 kg/m^3 (near the water surface) to 1 kg/m^3 (near the bed). The mud load, being the total amount of mud in the water column (of say 10 m), is in the range of L_{mud}= 1 to 10 kg/m^2. If this mud load is fully settled to the bed as a fluid mud layer with density of ρ_{dry}= 100 kg/m^3, the thickness of the fluid mud layer is $\delta_{fluidmud}= L_{mud}/\rho_{dry}$ = 0.1 m.
After slack water during spring tides, the high concentration fluid mud is normally re-entrained by the accelerating tidal currents. During lower energy conditions at neap tides, the fluid mud that forms during decelerating tidal conditions is typically not completely re-entrained; instead, the lutoclines rise in the water column during accelerating currents and then resettle during decelerating currents.
During the initial phase of fluid mud formation, hindered settling occurs as described above. Over longer time periods, the fluid mud consolidates to form a bed layer, which is called primary consolidation and associated dewatering.
A high-concentration fluid mud layer can easily move horizontally over an inclined bed. Turbulent and laminar fluid mud gravity flows are distinguished by a critical bed slope such that if the slope is too gentle, the downslope fluid mud flow cannot generate sufficient internal shear to overcome its inherently stable density

anomaly in order to generate turbulence. This critical slope is about 1° to 2°. Fluid mud on a slope greater than about 1° will accelerate downhill and, assuming the region of runout is long enough, generate enough internal shear to become turbulent.
If a fluid mud gravity flow moves down a constant slope of about one degree or less, then in the absence of externally imposed currents or waves, any turbulence present in the flow will decrease with time, and the lutocline will fall as sediment slowly settles. Fluid mud gravity flows are also likely to play an important role in estuaries over shorter distances, favoring fluid mud movement toward the deepest parts of estuaries, including deep navigation channels created and maintained by dredging
Management of sedimentation can be accomplished by various techniques, which are based on:
keep sediment out, keep sediment moving, or remove sediment once it has deposited.
This simple and useful classification can be adapted to fluid mud management techniques that accomplish: source control; formation control (including nautical depth definition) and removal.

5. Quasi-steady 1D mud transport model for tidal flow (TMUD.xls)

5.1 Definitions

The TMUD.xls model can be used to compute the depth-integrated suspended mud and fluid mud transport during tidal flow at a single location (point model). The fine silt/sand transport is included assuming that the silt/sand particles are washed out of the bed together with the mud particles ($p_{mud}+p_{silt\text{-}sand}=1$).
The velocities and mud concentrations are computed as a function of z and t; z=height above bed and t=time (fixed time step of 5 to 15 min). The grid points over the depth (50 points) are distributed according to an exponential function, as follows:

$$z=a[h/a]^{(k-1)/(N-1)} \qquad (5.1)$$

with: a= reference height above bed (input value), $h=h_o+\eta$= water depth, h_o= depth between bed and mean sea level, η= tidal water level, k= index number of point k, N= total number of grid points (=50).

5.2 Tidal water levels, flow and asymmetry

The tidal water level at each time t is represented, as:

$$\eta_{flood,t} = \eta_{flood,max} \sin\{\pi(t-\Delta T)/T_{flood}\} \quad \text{for } t < T_{flood} \qquad (5.2)$$
$$\eta_{flood,max} = f_a\,(H/2)$$
$$T_{flood} = (\eta_{ebb,max}/H)T$$
$$\eta_{ebb,t} = \eta_{ebb,max} \sin\{\pi(t-T_{flood}-\Delta T)/T_{ebb}\} \quad \text{for } t > T_{flood} \qquad (5.3)$$
$$\eta_{ebb,max} = -(1/f_a)(H/2)$$
$$T_{ebb} = (\eta_{flood,max}/H)T$$

with: H = tidal range tidal water level (input value); f_a= asymmetry factor (input value=1 tot 1.2, f_a=1 yields a symmetrical tide), T= tidal period (input value), ΔT= phase shift (seconds; velocity is ahead of water level), T_{flood}= flood period, T_{ebb}= ebb period.
The depth-averaged velocity at each time t is represented, as:

$$u_t = [u_r + u_{flood,max} \sin(\pi t/T_{flood})] \quad \text{for } t < T_{flood} \qquad (5.4)$$
$$u_{flood,max} = f_a\,(U_{max})$$
$$u_t = u_r + u_{ebb,max} \sin\{\pi(t-T_{flood})/T_{ebb}\} \quad \text{for } t > T_{flood} \qquad (5.5)$$
$$u_{ebb,max} = -1/f_a\,(U_{max})$$

with: u_t=depth-averaged velocity at time t (m/s), u_r= net tide-averaged and depth-averaged velocity = Q/(b h), b= flow width of channel (input value), h= water depth (input value),U_{max}= $(u_{flood,max}+u_{ebb,max})/2$ (input value),

5.3 Velocity profile

The vertical distribution of the velocity at each time t is represented, as:

$$u_{z,t} = (z/\delta_{fm})u_b \quad \text{for } z \le \delta_{fm} \qquad (5.6a)$$
$$u_{z,t} = [u_{res,z} + [(u_{river}+u_{tide})/(-1+\ln(h/z_o))]\ln(z/z_o)] \quad \text{for } z > \delta_{fm} \qquad (5.6b)$$
$$u_b = [u_{res,z=\delta fm} + [u_{river}+u_{tide})/(-1+\ln(h/z_o))]\ln(\delta_{fm}/z_o)] \qquad (5.6c)$$

with:
$u_{res,z}$= residual flow velocity due to horizontal salinity-induced density gradient based on Equation (3.5),
u_b= near-bed velocity at level $z=\delta_{fm}$,

δ_{fm}= thickness of fluid mud layer with concentrations larger than 5 to 10 kg/m^3 (input value; constant during tide), z= level above bed (m), h= water depth at time t = $h_o+\eta_t$ (m),
h_o= tide-averaged water depth (m),
η_t = tidal water level (m),
u_{tide} = depth-averaged flow velocity at time t due to tidal flow (m/s),
u_{river}= Q/(bh)= constant river velocity,
z_o= 0.033$k_{s,c}$ = zero-velocity level,
$k_{s,c}$ = current-related bed roughness (wave-current interaction is neglected).

The velocity inside the fluid mud layer is assumed to be linear, see Equation (5.6a).
The first part ($u_{res,z}$) of Equation (5.6b) represents the residual flow due to the density gradient and is constant in time. The depth-integration yields zero flow velocity. The second part represents the velocity profile due to tide and river flow.

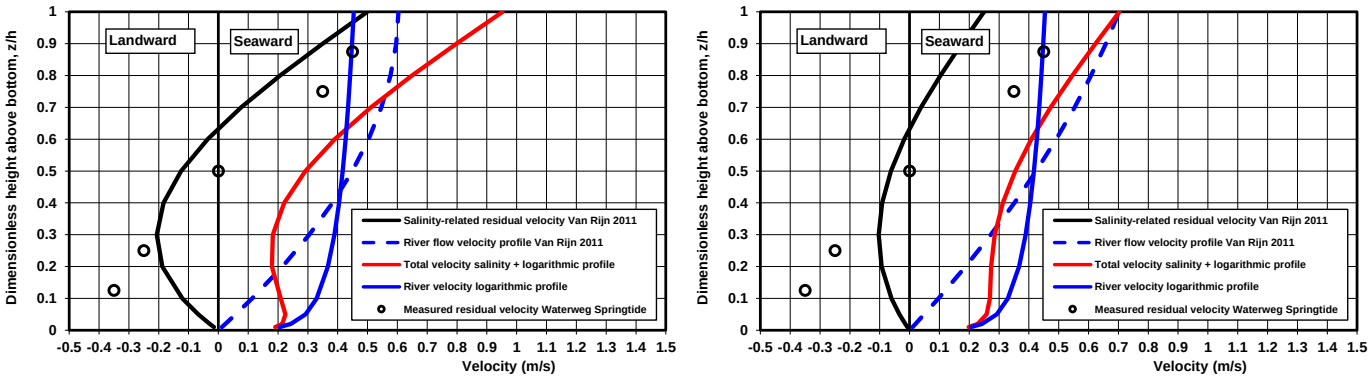

Figure 5.1 *River velocity plus salinity-induced residual flow velocity profile*
Left: γ= 0.005 and Right: γ= 0.01

Figure 5.1 show the residual flow velocity profile for h_o= water depth= 15 m, u_{tide}= 0 m/s, u_r= river velocity= 0.4 m/s, $k_{s,c}$=bed roughness= 0.1 m, ρ_{sea}= 1025 kg/m^3, $\partial\rho/\partial x$= 0.001. Two values of the γ-coefficient (0.005 and 0.01) have been used. Measured salinity-related residual flow velocities during the springtide of October 1975 in the Nieuwe Waterweg near Rotterdam are also shown. The agreement is best for γ=0.005. Two velocity profiles are shown for the steady river velocity. The logarithmic velocity profile is preferred and is implemented in the TMUD-model. The salinity-induced flow reduces the near-bed river flow velocity, but increases the river flow velocity near the water surface. The near-bed velocity at z≅ 0.15 h is used to compute the bed-shear stress.

5.4 Mud concentrations and transport

The sediment (mud) concentration balance equation for uniform flow (dh/dx and du/dx) reads as:

$$\partial c/\partial t - \partial c w_{mud}/\partial z - \partial(\varepsilon_s \partial c/\partial z)/\partial z = 0 \qquad (5.7a)$$

with: c= volume mud concentration (-), w_{mud}= settling velocity of suspended mud material (function of concentration c), ε_s= sediment mixing coefficient (function of concentration c).

Assuming w_{mud} and ε_s to be constant, it follows that:

$$\partial c/\partial t - w_{mud}\, \partial c/\partial z - \varepsilon_s\, \partial(\partial c/\partial z)/\partial z = 0$$
$$\Delta c/\Delta t - w_{mud}\, \Delta c/\Delta z - \varepsilon_s\, \Delta(\Delta c)/\Delta z^2 = 0$$

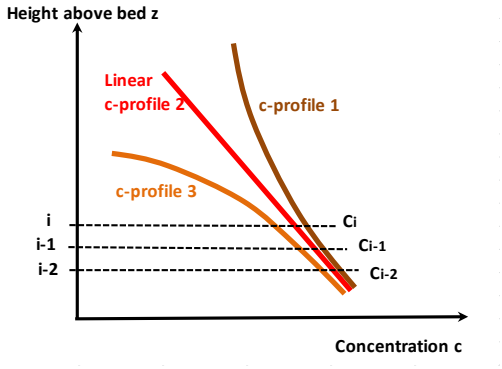

Figure 5.2 *Concentration profiles*

An explicit numerical approach yields:

$$W_{mud}\,\Delta c/\Delta z = -\,\varepsilon_s\,\Delta(\Delta c)/\Delta z^2 + \Delta c/\Delta t$$
$$\Delta c = -(\varepsilon_s/w_{mud})\,\Delta(\Delta c)/\Delta z + (\Delta z/w_{mud})\,(\Delta c/\Delta t)$$
$$c_i - c_{i-1} = -[(\varepsilon_s/(w_{mud}\,\Delta z)]\,\Delta(c_i - c_{i-1}) + (\Delta z/w_{mud})\,(\Delta c/\Delta t)$$
$$c_i - c_{i-1} = -[(\varepsilon_s/(w_{mud}\,\Delta z)]\,[\Delta c_i - \Delta c_{i-1}] + (\Delta z/w_{mud})\,(\Delta c/\Delta t)$$
$$c_i = c_{i-1} - [(\varepsilon_s/(w_{mud}\,\Delta z)]\,[(c_i - c_{i-1}) - (c_{i-1} - c_{i-2})] + (\Delta z/w_{mud})\,(\Delta c/\Delta t)$$

$$c_i = c_{i-1} - [(\varepsilon_s/(w_{mud}\,\Delta z)]\,[c_i - 2c_{i-1} + c_{i-2}] + [(\Delta z/w_{mud})\,(\Delta c/\Delta t)]$$

$$c_i = c_{i-1} - \alpha[c_i - 2c_{i-1} + c_{i-2}] + \beta(\Delta c/\Delta t)] \qquad (5.7b)$$

with: $\alpha = \varepsilon_s/(w_{mud}\,\Delta z)$ and $\beta = \Delta z/w_{mud}$; $\alpha>0$ and $\beta>0$.

The term $\alpha[c_i - 2c_{i-1} + c_{i-2}]$ is always positive for a decreasing concentration in vertical direction as given by c-profile 1 (see **Figure 5.2**). This term is zero for a linear concentration profile (second derivative of linear function is zero, see **Figure 5.2**). The term is negative for a concentration profile as given by the c-profile 3.

Equation (5.7b) can be further elaborated:

$$c_i = [(1+2\alpha)/(1+\alpha)]c_{i-1} - [\alpha/(1+\alpha)]c_{i-2} + [(\beta/((1+\alpha))\,(\Delta c/\Delta t)]$$

Using: $c_{i-2} = \gamma c_{i-1}$ with $\gamma > 1$, it follows that

$$c_i = [(1+2\alpha-\alpha\gamma)/(1+\alpha)]c_{i-1} + [(\beta/(1+\alpha))(\Delta c/\Delta t)] \qquad (5.7c)$$
Term A Term B

The term $(1+2\alpha-\alpha\gamma)/(1+\alpha)$ will be between 0 and 1 as long as γ is between 1 and 2; $\gamma=1$ yields $c_{i-2} = c_{i-1}$ and $\gamma=2$ yields $c_i = [1/(1+\alpha)]c_{i-1}$. For $\gamma>2$, term $(1+2\alpha-\alpha\gamma)/(1+\alpha)$ may become negative for large values of α resulting in negative concentrations.
The requirement $1<\gamma<2$ means that the vertical grid size should be very small (in the range of 0.001 to 0.01 m) which is a common feature of an explicit numerical scheme.

The values of the Terms A and B of Equation (5.7c) have been estimated in **Table 5.1**, which shows that the concentration time effect (Term B) is relatively small near the top of the fluid mud layer. The concentration time effect is more important near the water surface where the settling velocity is relatively small (small concentrations and limited flocculation). The vertical grid size should be sufficiently small (<0.01 m near the bed and <0.1 m near the water surface).

At the bottom of the fluid mud layer with concentrations > 100 kg/m^3 where consolidation processes take place, the time effect is of crucial importance as the effective settling velocity is extremely small (almost zero) due to hindered settling.

Term		**Dimension**	**Near the bottom (top of fluid mud layer)**	**Near the water surface**
Concentration	c	kg/m^3	1 to 100	0.1 to 1
Vertical grid size	Δz	m	0.01	0.1
Time gradient concentration (variation of concentration over 3 hours)	$\Delta c/\Delta t$	kg/(m^{3}s)	100/10000 = 0.01	1/10000 = 0.0001
Settling velocity	w_{mud}	m/s	0.001 (flocculated)	0.0001
Mixing coefficient	ε_s	m^2/s	0.001	0.001-0.01
α-term	$\alpha = \varepsilon_s/(w_{mud}\,\Delta z)$	-	100	100-1000
β-term	$\beta = \Delta z/w_{mud}$	s	10	1000
α-β term	$\beta/(1+\alpha)$	s	0.1	1-10
Term A: $[(1+2\alpha-\alpha\gamma)/(1+\alpha)]c_{i-1}$ with γ=1.9 yields: $[(1+0.1\alpha)/(1+\alpha)]c_{i-1} \cong$	$0.1\ c_{i-1}$	kg/m^3	0.1	0.01
Term B:	$(\beta/(1+\alpha))(\Delta c/\Delta t)$	kg/m^3	0.001	0.001

Table 5.1 *Comparison of concentration terms for tidal flow conditions*

Neglecting the $\partial c/\partial t$-term of Equation (5.7a), the mud concentration profile at each time t is given by:

$$c w_{mud} + \varepsilon_s dc/dz = 0 \qquad (5.7d)$$

with: c= volume mud concentration (-), w_{mud}= settling velocity of suspended mud material (function of concentration c), ε_s= sediment mixing coefficient (function of concentration c).

Since the settling velocity and the sediment mixing coefficient are both dependent on the concentration, Equation (5.7d) cannot be solved analytically. Therefore, Equation (5.7d) is discretized as (explicit approach):

$$c_i w_{mud} + \varepsilon_s \Delta c/\Delta z = 0$$
$$c_i w_{mud} + \varepsilon_s (c_i - c_{i-1})/\Delta z = 0$$
$$c_i w_{mud} + (\varepsilon_s/\Delta z)\, c_i = (\varepsilon_s/\Delta z) c_{i-1}$$
$$c_i [w_{mud} + (\varepsilon_s/\Delta z)]_i = (\varepsilon_s/\Delta z) c_{i-1}$$
$$c_i [w_{mud}\,\Delta z/\varepsilon_s + 1)] = (1)\, c_{i-1}$$
$$c_i = c_{i-1} [1 + w_{mud}\,\Delta z/\varepsilon_s)]^{-1} \qquad (5.7e)$$

or

$$c_i \cong c_{i-1} [1 - w_{mud}\,\Delta z/\varepsilon_s] \qquad \text{for } w_{mud}\,\Delta z/\varepsilon_s < 0.1 \qquad (5.7f)$$

Equations (5.7e,f) yield a decreasing concentration in vertical direction as the term $w_{mud}\,\Delta z/\varepsilon_s$ is positive. The term $w_{mud}\,\Delta z/\varepsilon_s$ should remain smaller than 0.1. Thus: $w_{mud}\,\Delta z/\varepsilon_s < 0.1$ or $\Delta z < 0.1\,\varepsilon_s/w_{mud}$.

Using: $\varepsilon_s = 0.001$ m^2/s and $w_{mud} = 0.001$ m/s near the bed and $w_{mud} = 0.0001$ m/s near the water surface, it follows that the vertical grid size $\Delta z < 0.1$ m near the bed and $\Delta z < 1$ m near the water surface.

The boundary condition at the bed is represented by the reference bed concentration $c_{a,mud}$, as follows:

$$c_{a,mud} = p_{mud}[(c_{a,mud,o} + \alpha_{mud}(\tau_{b,cw}-\tau_{b,cr,e})/\tau_{b,cr,e})^n] \qquad (5.8)$$

with:
α_{mud}= erosion coefficient (input value; range of 0.0001 to 0.1),
p_{mud}= percentage of mud of top layer of bed,
$c_{a,mud,o}$= constant background concentration near bed (input value; range of volume concentration 0.005 to 0.5 or mass concentration 10 to 200 kg/m^3),
$\tau_{b,cr,e}$= critical bed-shear stress for erosion (input value),
$\tau_{b,cw} = \tau_{b,c}+\tau_{b,w}$= bed-shear stress due to current and waves,
n= power of bed-shear stress (range 1 to 1.5; input value).

The effect of the time lag on the mud concentrations is represented by applying an exponential adjustment of the near-bed concentration ($dc_{a,mud}/dt = -\gamma_{mud}\,(c_{a,mud,t}-c_{a,mud,t,eq})$), resulting in the actual bed concentration $c_{a,mud,t}$ at time t:

$$c_{a,mud,t} = c_{a,mud,t-\Delta t} + dc_{a,mud} \qquad (5.9)$$
$$c_{a,mud,t} = c_{a,mud,t-\Delta t} + [-\gamma_{mud}\,(c_{a,mud,t}-c_{a,mud,t,eq})\Delta t] \qquad (5.10)$$
$$c_{a,mud,t} = [1/(1 + \gamma_{mud}\,\Delta t)][c_{a,mud,t-\Delta t} + \gamma_{mud}\,\Delta t\, c_{a,mud,t,eq}] \qquad (5.11)$$

with:
Δt= time step (5 to 15 min), $c_{a,mud,t-\Delta t}$= bed concentration at previous time, $c_{a,mud,t,eq}$= equilibrium bed concentration at time t, γ_{mud} = adjustment parameter $\cong 0.0001$ (input value in range of 0.00005 to 0.0002).

The time lag effect of the mud concentration can be manipulated by using the γ_{mud}-coefficient. A value of $\gamma_{mud} > 0.01$ yields a near-bed concentration almost equal to the equilibrium value.

Figure 5.3 shows the near-bed concentration for $\gamma_{mud} = 0.0003$ and $\gamma_{mud} = 0.0001$. A smaller γ_{mud}-coefficient yields a smaller oscillation amplitude of the near-bed concentration.

The lag period of the peak concentration with respect to the peak tidal flow velocity is of the order of 2 hours for $\gamma_{mud} = 0.0001$. Input values are taken from the Amazon example in Section 5.6

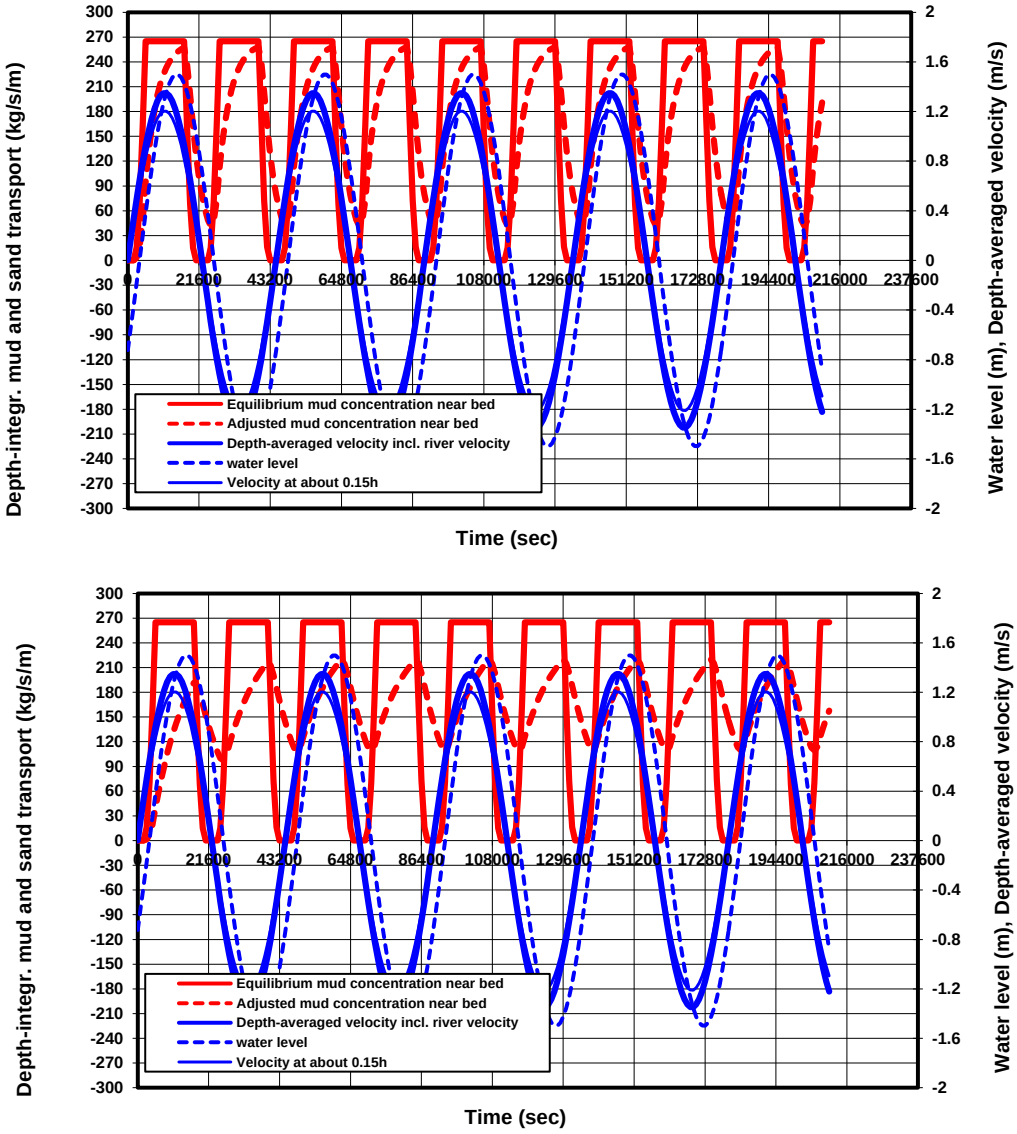

Figure 5.3 *Near-bed concentration for γ_{mud}= 0.0003 (upper) and γ_{mud}= 0.0001 (lower)*

The bed-shear stresses are represented as:

$$\tau_{b,c} = \rho_w \kappa^2 u_b^2/[\ln(30z_b/k_{s,c})]^2 \quad (5.12a)$$

$$\tau_{b,c} = 0.125\ \rho_w f_c (u_c)^2 \quad (5.12b)$$

$$\tau_{b,w} = 0.25\ \rho_w f_w (U_w)^2 \quad (5.13)$$

with:
u_b=near-bed velocity at z_b=0.2h; h=water depth,
$U_w = (2\pi/T_p)A_w$=peak orbital velocity (linear wave theory),
A_w= peak orbital excursion,
T_p= peak wave period,
$f_w = \exp(-6+5.2(A_w/k'_{s,w}))$= wave-related friction coefficient,

$f_c=0.24/(\log(12h/k'_{s,c}))^2$= current-related friction coefficient,
H_s= significant wave height,
$k'_{s,c}$= current-related roughness of flat bed surface (range of 0.0001 to 0.001 m),
$k'_{s,w}$= wave-related roughness of flat bed surface (range of 0.0001 to 0.001 m),
ρ_s= sediment density (input value), ρ_w= fluid density (input value).
Equation (5.12a) is used in Equation(5.8).

The concentration-dependent mud settling velocity is represented as:

$$w_{mud} = \exp[\alpha_1 \ln(c) + \alpha_2 - \alpha_3]; \quad \text{for flocculation range } c \leq 0.0025 \qquad (5.14a)$$

$$\alpha_1 = 0.182 \ln(w_{mud,max}/w_{mud,min})$$
$$\alpha_2 = 2.09 \ln(w_{mud,max})$$
$$\alpha_3 = 1.09 \ln(w_{mud,min})$$

$$w_{mud} = w_{mud,max}(1-c)^4 \quad \text{for hindered settling range } c > 0.0025 \qquad (5.14b)$$

with:
$w_{mud,max}$= maximum settling velocity at c=0.0025 ($w_{mud,max}$ =0.0005 to 0.003 m/s or 0.5 to 3 mm/s; input value),
$w_{mud,min}$=minimum settling velocity at c=0.00001 ($w_{mud,min}$=0.00005 to 0.0001 m/s or 0.05 to 0.1 mm/s; input value).
The settling velocity at height z_k is determined by using the concentration values at height z_{k-1}.

Some characteristic values of the settling velocity w_{mud} are:

c=0.000025 (=0.066 kg/m^3)	w_{mud}=0.000145 m/s	= 0.145 mm/s
c=0.00025 (=0.66 kg/m^3)	w_{mud}=0.00038 m/s	= 0.38 mm/s
c=0.0025 (=6.6 kg/m^3)	w_{mud}=0.001 m/s	= 1 mm/s
c=0.025 (=66 kg/m^3)	w_{mud}=0.0009 m/s	= 0.9 mm/s
c=0.1(=265 kg/m^3)	w_{mud}=0.00066 m/s	= 0.66 mm/s

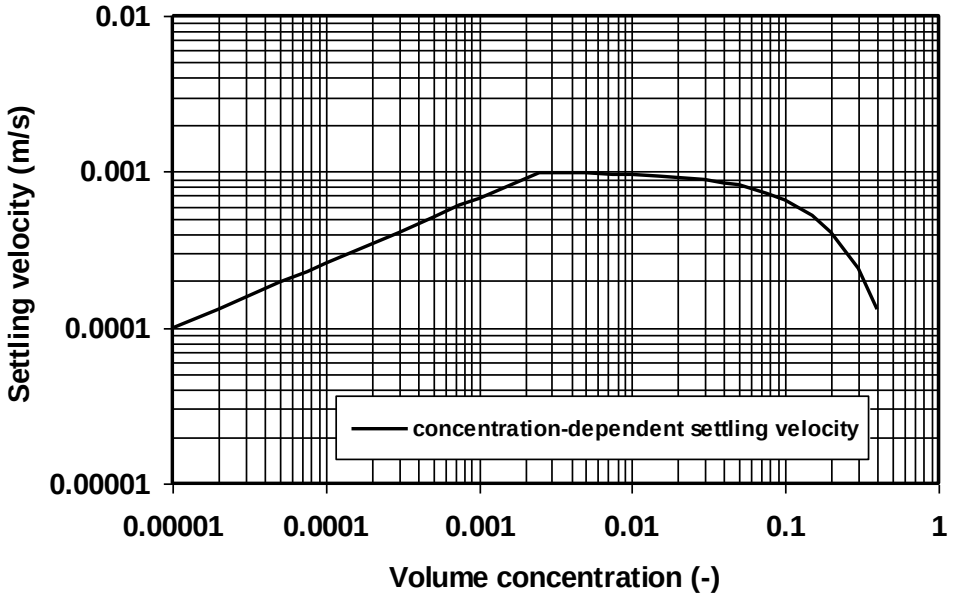

Figure 5.4 *Settling velocity as function of volume concentration; flocculation range for c<0.0025 and hindered settling range for c>0.0025; $w_{mud,max}$=0.001 m/s, $w_{mud,min}$=0.0001 m/s*

Equation (5.14) using $w_{mud,max}$=0.001 m/s and $w_{mud,min}$=0.0001 m/s, is shown in **Figure 5.4**.

Using a concentration-dependent settling velocity, the transport of mud < 32 μm can be represented by one single fraction. Using a constant settling velocity, it may be better to use two fractions (4-16 μm and 16-32 μm).

The sediment mixing coefficient distribution in the presence of fluid mud near the bed is represented by a linear distribution, as follows:

$\varepsilon_s = \phi_d \, \varepsilon_b$ for $z \leq \delta_{fm}$ (5.15a)

$\varepsilon_s = \phi_d \, [\varepsilon_b + (\varepsilon_{max} - \varepsilon_b)(z-\delta_{fm})/(0.5h-\delta_{fm})]$ for $\delta_{fm} < z < 0.5h$ (5.15b)

$\varepsilon_s = \phi_d \, [(h-z)/(0.5h)] \, \varepsilon_{max}$ for $z \geq 0.5h$ (5.15c)

$\varepsilon_{max} = 0.05 \, \gamma_{mid} \, u_{*,cw} \, h$

$\varepsilon_b = 0.5 \, \gamma_{bed} \, \varepsilon_{max}$

$\varepsilon_{min} = 0.001 \; m^2/s$

with:
δ_{fm} = thickness of fluid mud layer (input value),
ε_b= sediment mixing coefficient in fluid mud layer,
ε_{max}= maximum sediment mixing coefficient at z/h=0.5,
h= water depth, $u_{*,cw} = (u_{*,c}^2 + u_{*,w}^2)^{0.5}$= bed-shear velocity due to current and waves,
$u_{*,c} = (\tau_{b,c}/\rho_w)^{0.5}$= current-related bed-shear stress,
$u_{*,w} = (\tau_{b,w}/\rho_w)^{0.5}$= wave-related bed-shear stress,
$\gamma_{mid}, \gamma_{bed}$ = calibration coefficient (default=1),
ϕ_d= turbulence damping coefficient (function of Richardson number),
$Ri = [-(g/\rho)][d\rho/dz]/[(du/dz)^2] = [-(\rho_s-\rho_w)g/((\rho_w+(\rho_s-\rho_w)c)][dc/dz]/[(du/dz)^2]$ = Richardson number (salinity and temperature effects on the vertical density gradient are neglected),
$\rho = \rho_s c + (1-c)\rho_w$= fluid-sediment mixture density,
c= volume concentration,
ε_{min}= 0.001 m^2/s= minimum value at slack tide conditions.

The concentration and velocity gradients are determined by using the values at heights z_{k-1} and z_{k-2}.

The damping function is expressed as (Munk and Anderson 1948):

$$\phi_d = (1 + \alpha_d \, 2Ri^{0.5})^{-1} \quad (5.16)$$

with: α_d= calibration coefficient (default=1; in range of 0 to 2), Ri=Richardson number (-).

The depth-integrated mud transport rate q_{mud} at each time t is computed as:

$$q_{mud} = \int_a^h (uc) \, dz \quad (5.17)$$

The tide-integrated mud transport rates are computed as:

$$Q_{mud,pos} = \int (q_{mud,pos}) \, dt, \quad Q_{mud,neg} = \int (q_{mud,neg}) \, dt, \quad Q_{mud,net} = Q_{mud,pos} + Q_{mud,neg} \quad (5.18)$$

Computed mud concentrations ($c_{mud}=q_s/q$) of the TMUD-model are shown in **Figure 5.3** for a water depth of h= 10 m, settling velocity $w_{s,o}$= 0.005 m/s, $k_{s,c}$= 0.0001 m, $\tau_{cr,mud}$= 0.05 n/m^2. Two values of the mud coefficient have been used: α_{mud}= 0.003 and 0.02. Both black curves of computed mud concentrations are within the variation range of the measured values.

5.5 Suspended sand load and transport

In the case of mud-sand mixtures (percentage mud >70%), the suspended sand load can be determined by assuming that the top layer of the bed is homogeneously mixed and that the sand particles are eroded together with the mud particles. The assumption of a homogeneous top layer may not be realistic, as often a layered structure is observed (segregation effect).
The suspended mud load can be determined as:

$$L_{mud} = \int_a^h (c_{mud})dz \qquad (5.19)$$

The corresponding layer thickness of eroded mud is:

$$\Delta_s = L_{mud}/(p_{mud}\ \rho_{b,mud}) \qquad (5.20)$$

with: p_{mud}= percentage of mud of top layer of bed, $\rho_{b,mud}$= bulk density of mud fraction (incl. pores; about 500 to 1000 kg/m^3).
The amount of sand in this eroded mud layer is:

$$L_{sand} = p_{sand}\ \rho_{b,sand}\ \Delta_s = (p_{sand}/p_{mud})\ (\rho_{b,sand}/\rho_{b,mud})\ L_{mud} \qquad (5.21)$$

with: p_{sand}= percentage of sand of top layer of bed, $\rho_{b,sand}$= bulk density of sand fraction (incl. pores; about 1000 to 1600 kg/m^3).
The suspended sand load is also defined by:

$$L_{sand} = \int_a^h (c_{sand})dz = c_{a,sand}\ \int_a^h (f_z)\ dz \qquad (5.22)$$

with: $f_z=[((h-z)/z)(a/(h-a))]^{ZM}$, $ZM=w_{sand,o}/(\kappa u_{*,cw})$= suspension number of sand, $w_{sand,o}$= fall velocity of individual sand particles, $u_{*,cw}$= bed-shear velocity due to currents and waves.

The reference concentration of silt/sand can now be determined as:

$$c_{a,sand} = L_{sand}/\int_a^h (f_z)\ dz = [(p_{sand}/p_{mud})\ (\rho_{b,sand}/\rho_{b,mud})\ L_{mud}]/[\int_a^h (f_z)\ dz] \qquad (4.4.23)$$

The maximum reference sand concentration is given by:

$$c_{a,sand,max} = 0.015\ p_{sand}(d_{50}/a)\ (T)^{1.5}\ (D_*)^{-0.3} \qquad (5.24)$$

with:
d_{50}= median particle diameter,
$D_*= d_{50}((s-1)g/\nu^2)^{0.333}$= dimensionless particle parameter,
$T=(\tau_b'-\tau_{b,cr,pure\ sand})/\tau_{b,cr,pure\ sand}$= dimensionless bed-shear stress parameter,
$\tau_{b,cr,pure\ sand}$= critical bed-shear stress of sand (input value; Shields value),
$\tau_b'= \tau'_{b,c}+\tau'_{b,w}$= bed-shear stress due to current and waves (efficiency factors are assumed to be 1 for a flat bed),
$s=\rho_s/\rho_w$= relative density,
ν= kinematic viscosity coefficient,
ρ_s= sediment density (input value),
ρ_w= fluid density (input value).

The sand transport can be determined from: $q_{sand} = \int_a^h (u\ c_{sand})\ dz$ (5.25)

5. 6 Example computations

5.6.1 Amazone mouth, Brasil

Mud concentrations have been measured at 2 stations (OS2 and CN, see **Figure 5.5**) in the mouth of the Amazon river, Brasil (Vinzon and Mehta 2003). Due to the large river runoff, flow and sediment dynamics are dominated by estuarine processes up to a depth of about 100 m. Both stations are located in the lee of Cabo Norte shoal and are sheltered from direct impact of the river runoff. The mean depth at the site is about 16 to 18 m. The spring tidal range is about 3.1 m. A suspended sediment profiler was used to collect depth-profile data of the current by electromagnetic currentmeter and suspended sediment concentrations by optical backscatter instruments (OBS). The lowest measurement elevation was 0.25 m above the level at which the profiler rested on the bed. **Figure 5.6** shows measured concentrations and flow velocities over the water depth at peak tidal flow; the data of Figure 5.6 were composed from the measured data of Vinzon and Mehta (2003). The following features can be observed:

- lower layer (hindered settling layer or hyperpycnal layer) of about 2 m thick with high concentrations in the range of 10 to 200 kg/m^3; hindered settling is the dominant process; upward mixing by turbulence is almost nil as the turbulence is strongly damped; turbulence collapse commencces for concentrations > 40 kg/m^3; the upper boundary of this layer is the lutocline (sharp almost horizontal interface with large concentration gradient); velocity profile is almost linear and is dominated by viscosity;
  majority of the sediment load is transported in this layer;
- well-mixed upper layer of small concentrations < 1 kg/m^3 (dilute suspension layer); settling velocities are relatively small in this layer; flocculation is minor; the suspended sediment is largely finegrained with a median (dispersed) grain size of about 3 μm;
- intermediate layer (flocculation layer) with concentrations between 1 and 10 kg/m^3; settling velocities are relatively large.

The results of an example computation assuming a pure mud bed (no sand) for station in the mouth area of the Amazon River (Brasil) are shown in **Figures 5.6** to **5.11.**

The input values of Case 2 are:
p_{mud}=1, p_{sand}=0, h= 17 m,
η_{peak} = 1.5 m (Tidal range= 3 m), H_s= 0 m, T_p= 0 s,
u_r= 0 m/s (river velocity), $u_{c,peak}$= 1.35 m/s, T= 45000 s, φ=1 hours, dρ/dx=0,
$w_{mud,max}$= 0.002 m/s, $w_{mud,min}$= 0.0005 m/s,
$k'_{s,c,surface}$= 0.0001 m, $k_{s,c,velocity\ profile}$= 0.1 m, $k'_{s,w}$=0.0001 m,
ρ_s= 2650 kg/m^3, ρ_w= 1025 kg/m^3, ν= 0.000001 m^2/s,
$\tau_{b,cr,mud}$= 0.1 N/m^2, a= 0.1 m, δ_{fm}= 2 m,
Δt= 900 s, α_{mud}= 0.02, γ_{mix}= 0.3,
α_d= 1 (Ri-approach for damping function), n=1.

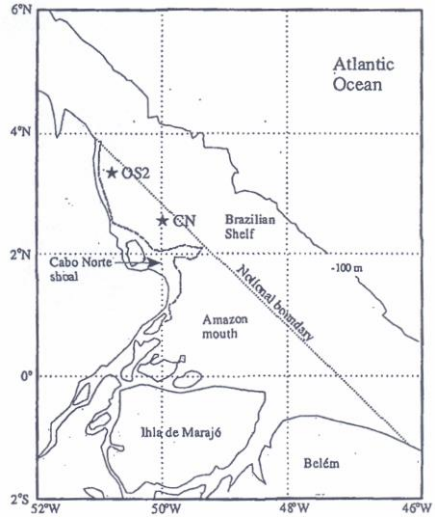

Figure 5.5 *Amazon site, Brasil*

The coefficient of the bed concentration was fitted (α_{mud}= 0.02) to obtain the best agreement of computed and measured values in the near-bed region. The mud transport rates are shown in **Table 5.2** (Cases 1 to 5) for various settings.
The settling velocity was represented by a constant value of $w_{mud,max}$=0.002 m/s (Case 1) and by a concentration-dependent settling velocity (Case 2) between $w_{mud,max}$=0.002 m/s and $w_{mud,min}$=0.0005 m/s.

Figure 5.6 shows the tidal variation of the computed depth-integrated mud transport rates for a constant settling velocity (Case 1).
Figure 5.7 shows computed and measured concentrations at peak tidal velocity for Case 1. The best agreement of measured and computed concentrations is obtained for a constant settling velocity (Case 1) of 0.002 m/s. A fluid mud layer is present with a thickness of the order of 2 m (concentrations > 10 kg/m^3). The concentrations in the upper part of the water depth and hence the depth-integrated mud transport are much larger, when the damping coefficient is reduced (α_d= 0.5, Case 3).

Figure 5.8 shows the tidal variation of the computed depth-integrated mud transport rates for a concentration-dependent settling velocity (Case 2).
Figure 5.9 shows computed and measured concentrations at peak tidal velocity for Case 2.
Figure 5.10 shows computed concentration profiles for peak flood and peak ebb velocities for Case 2.
Figure 5.11 shows the computed concentration profile with smaller concentrations at slack tide with velocities smaller than 0.001 m/s (Case 2).

Settings	**Depth-integrated mud transport (kg/s/m) at peak tidal (positive) flood flow**	**Depth-integrated mud transport (kg/s/m) at peak tidal (negative) ebb flow**	**Tide-integrated mud transport (ton/m)** **Positive (landward)**	**Negative (seaward)**	**Net**
Case 1; constant settling velocity=0.002 m/s, damping coefficient α_d= 1	45	-35	410	-325	85
Case 2; concentration-dependent settling velocity 0.0005 to 0.002 m/s, damping coefficient α_d= 1	55	-40	510	-410	100
Case 3; concentration-dependent settling velocity 0.0005 to 0.002 m/s, damping coefficient α_d= 0.5	140	-110	1320	-1070	250
Case 4; concentration-dependent settling velocity 0.0005 to 0.002 m/s, damping coefficient α_d= 1.5	30	-25	300	-240	60
Case 5; concentration-dependent settling velocity 0.0005 to 0.002 m/s, damping coefficient α_d= 1; asymmetric tide f_A= 1.1	70	-30	565	-315	250
Measured	30				

Table 5.2 *Computed and measured mud transport rates for Amazon mouth station*

For all Cases (1 to 4), the mud transport rates during the phase with negative ebb velocities and low tide (η_{peak} = 1.5 m) are somewhat smaller (15% smaller water depth, 2% larger bed-shear stresses, 13% smaller mixing coefficients) than those during high tide (see **Figures 5.6** and **5.8**), resulting in a small positive transport rate in landward direction during the full tidal cycle (see **Table 5.2**).
Using a concentration-dependent settling velocity (Case 2), the concentrations in the upper part of the concentration profile are somewhat larger resulting in larger transport rates, which may be caused by

overprediction of the sediment mixing coefficients (somewhat too large). The settling velocity in the upper part of the flow may also be somewhat too large. If the tide is asymmetric ($u_{max,flood}$=1.48 m/s, $u_{max,eb}$=1,22 m/s; Case 5) , the net tide-integrated transport increases to 200 ton/m., see **Table 5.2**.
The agreement between measured and computed velocity profiles in the fluid mud layer, based on a linear velocity profile, is quite good (see **Figures 5.7** and **5.9**).

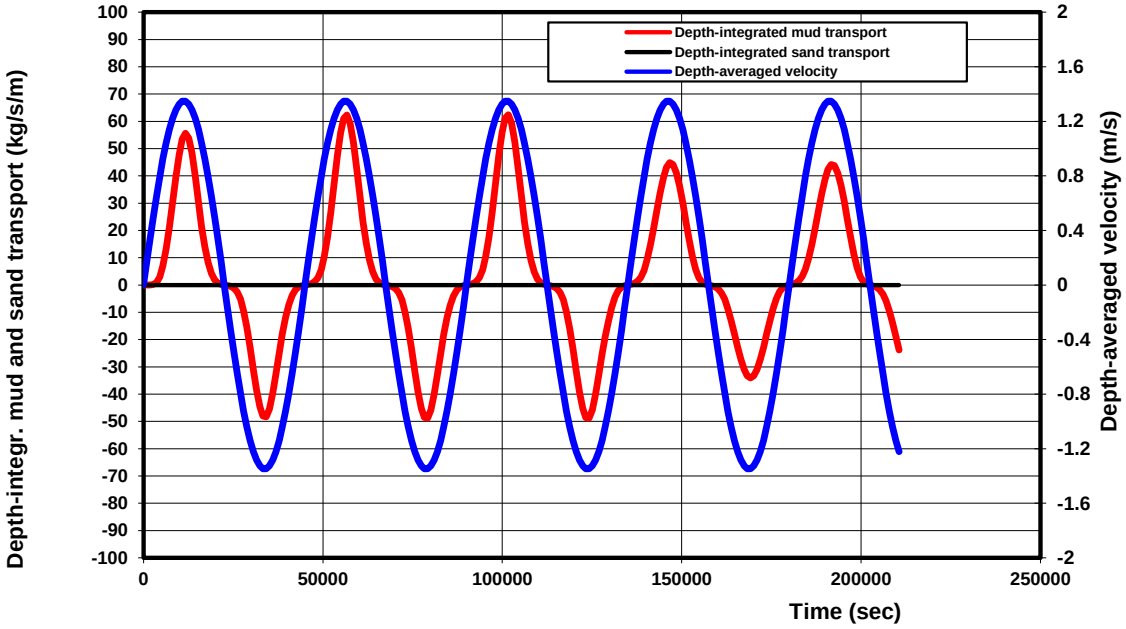

Figure 5.6 *Computed depth-integrated mud transport and depth-averaged flow velocity; constant settling velocity $w_{mud,max}$=0.002 m/s; damping coefficient α_d= 1; p_{mud}= 1 (Case 1)*

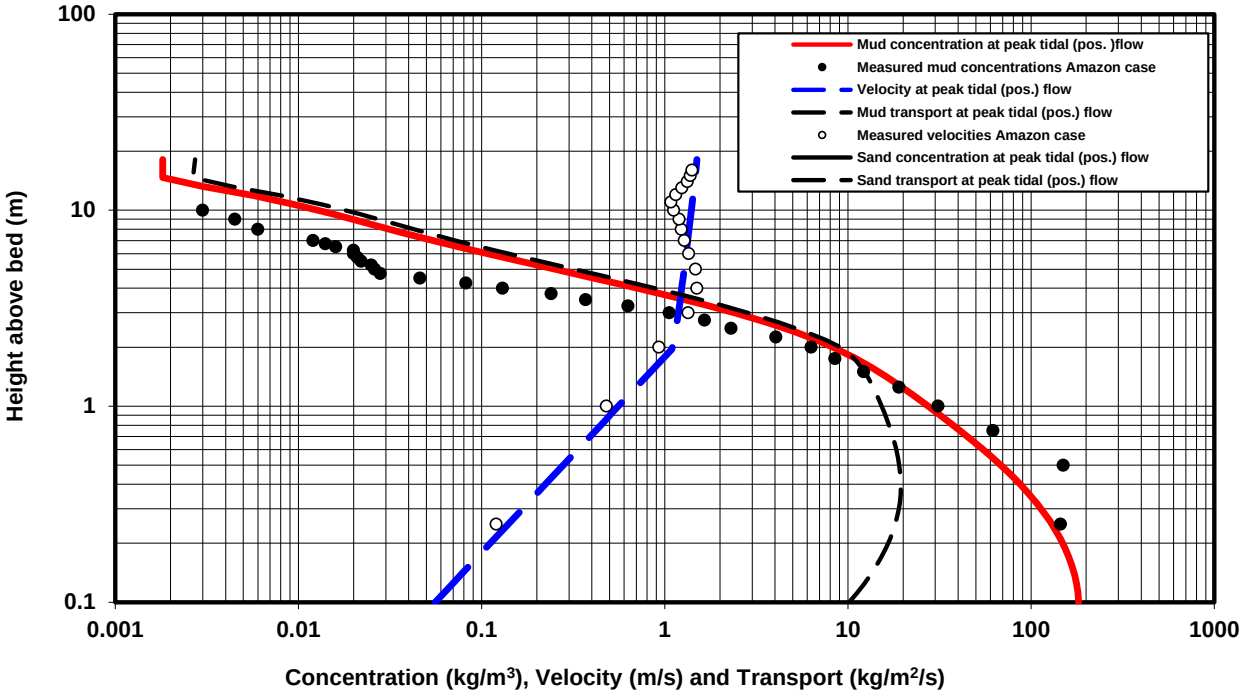

Figure 5.7 *Measured and computed velocity, mud concentration and mud transport over the depth at peak flood flow for the Amazon mouth; computed values based on constant settling velocity of $w_{mud,max}$=0.002 m/s; damping coefficient α_d= 1; p_{mud}=1 (Case 1)*

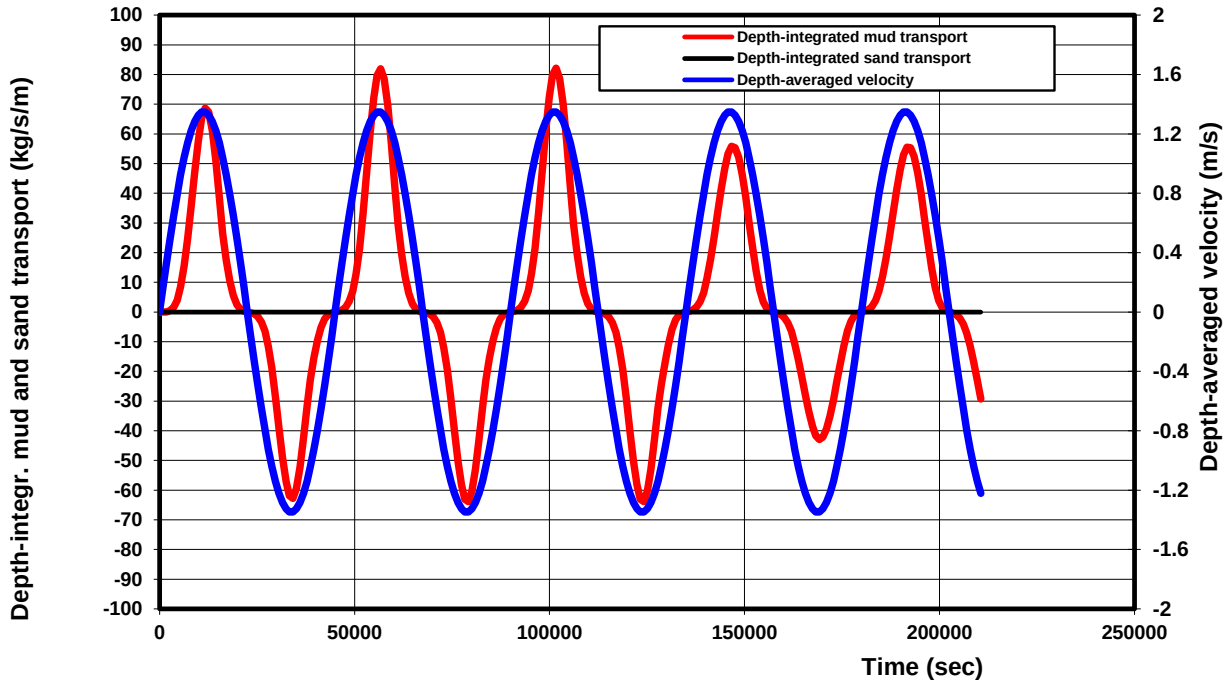

Figure 5.8 *Computed depth-integrated mud transport and depth-averaged flow velocity; concentration-dependent settling velocity $w_{mud,}$=0.0005 to 0.002 m/s; damping coefficient α_d= 1; p_{mud}= 1 (Case 2)*

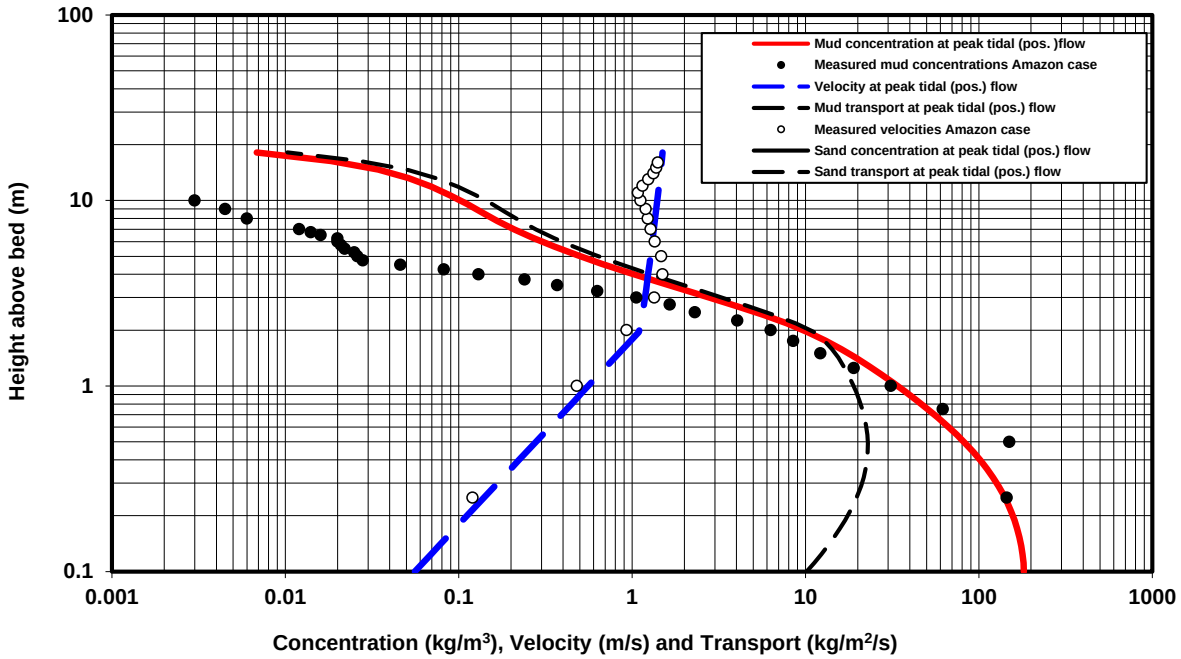

Figure 5.9 *Measured and computed velocity, mud concentration and mud transport over the depth at peak flood flow for the Amazon mouth; computed values based on concentration-dependent settling velocity of w_{mud}=0.0005 to 0.002 m/s; damping coefficient α_d= 1; p_{mud}= 1 (Case 2)*

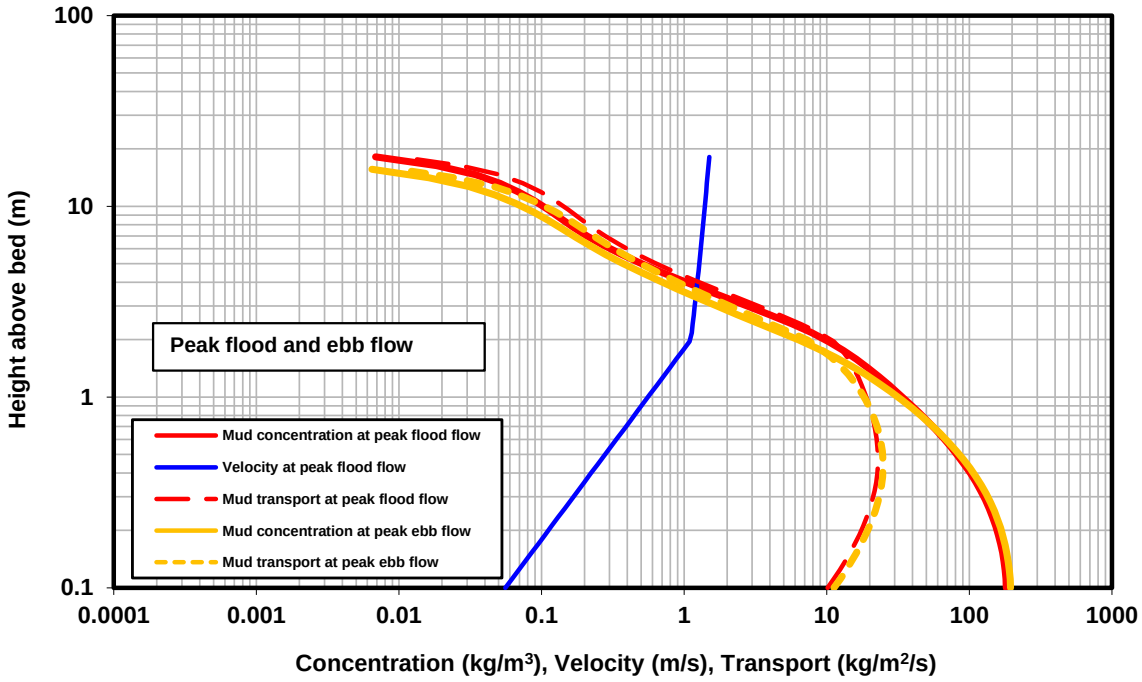

Figure 5.10 *Computed velocity, mud concentration and mud transport over the depth at peak flood and ebb flow for the Amazon mouth; computed values based on concentration-dependent settling velocity of w_{mud}=0.0005 to 0.002 m/s; damping coefficient α_d= 1; p_{mud}= 1 (Case 2)*

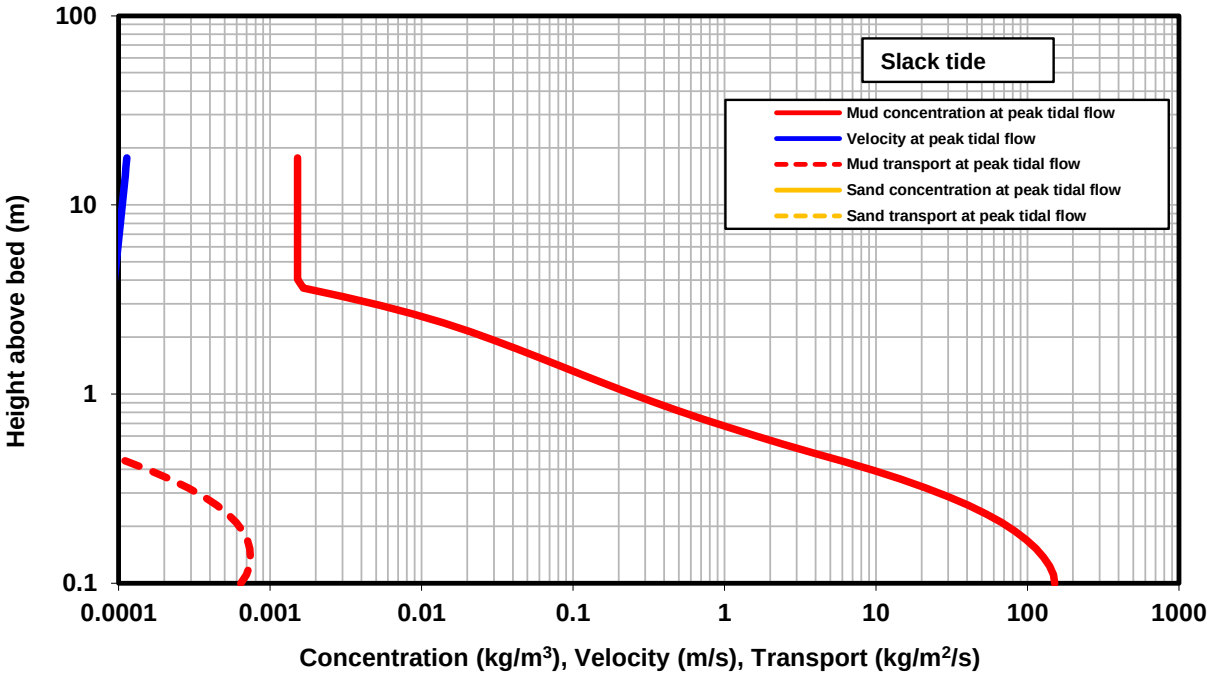

Figure 5.11 *Computed velocity, mud concentration and mud transport over the depth at slack tide for the Amazon mouth; computed values based on concentration-dependent settling velocity of w_{mud}=0.0005 to 0.002 m/s; damping coefficient α_d= 1; p_{mud}= 1 (Case 2)*

5.6.2 Tidal Ems river, Germany

The Ems-Dollard estuary consists of the tidal River Ems (Figure 5.5), which measures about 65 km from Hebrum weir to the mouth of the river at the large tidal Dollard bay. Upstream, near Hebrum, the width of the river measures about 60 m, increasing to about 120 m near Papenbrug and around 600 m near the river mouth. The shallow and very muddy Dollard forms part of the Wadden Sea complex situated at the border between The Netherlands and Germany. The major part of the Wadden Sea and Ems-Dollard estuary seabed is fairly sandy, with exceptions, in particular in the shallow areas along the mainland. However, the seabed of the Dollard, the large tidal basin at the head of the estuary, and the Ems River are (very) muddy. The Ems River is largely situated on German territory. The data of location A (river width of about 200 m) south of the city of Leer are taken from Winterwerp (2011). The tidal data and depth-integrated mud transport rates are shown in **Figure 5.12**. The tidal range was about 2.8 m during the survey period. The salinity at location A was very small (<0.5 ppt). The peak flood velocity was about 1 m/s, the peak ebb velocity was about 0.8 m/s. The flood period was about 5.5 hours with an acceleration duration of about 1 hour. This type of asymmetry with time cannot be represented by the TMUD-model, which is based on sinusoidal tidal velocities. The depth-averaged mud concentration was about 0.6 kg/m^3 during flood. The net tide-integrated mud transport based on measured mud concentrations is about 8500 kg/m/tide.

The basic data used for the TMUD-mdel are:
p_{mud}=1, p_{sand}=0, h= 7 m,
η_{peak} = 1.4 m, H_s= 0 m, T_p= 0 s,
u_r= 0 m/s (river velocity; no river discharge), $u_{c,peak}$= 0.9 m/s, asymmetry= 1.1, T= 45000 s, φ=3 hours (phase lead velocity), $d\rho/dx$=0 (fluid density gradient),
$w_{mud,max}$= 0.002 m/s, $w_{mud,min}$= 0.0005 m/s,
$k'_{s,c,surface}$= 0.0001 m, $k_{s,c,velocity\ profile}$= 0.1 m, $k'_{s,w}$=0.0001 m,
ρ_s= 2650 kg/m^3, ρ_w= 1005 kg/m^3, ν= 0.000001 m^2/s, $\tau_{b,cr,mud}$= 0.1 N/m^2, a= 0.1 m, δ_{fm}= 1 m, Δt= 900 s, α_{mud}= 0.003, γ_{mud}= 0.0001, γ_{mix}= 0.3, α_d= 1 (Ri-approach for damping function), n=1.

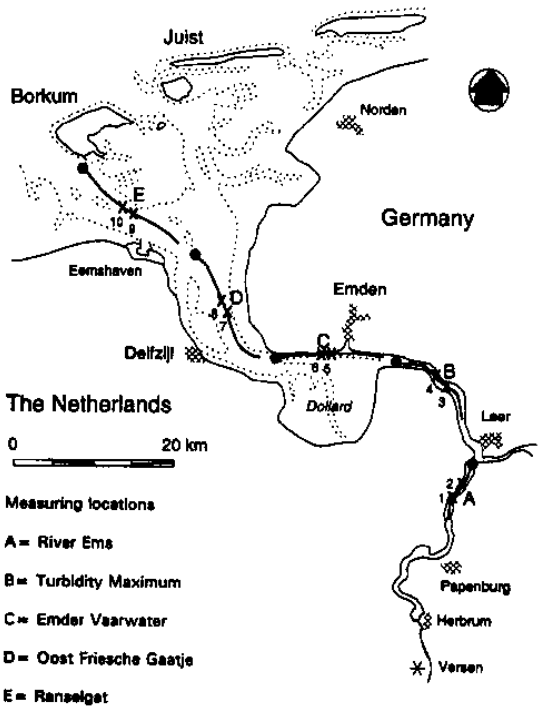

Figure 5.12 *Ems river, Germany*

The settling velocity was represented by a concentration-dependent settling velocity between $w_{mud,max}$= 0.002 m/s and $w_{mud,min}$=0.0005 m/s to represent the effects of flocculation and hindered settling. Turbulence damping was represented by a damping factor related to local Richardson number.
The coefficient of the bed concentration was fitted (α_{mud}= 0.003) to obtain the best agreement of computed and measured mud transport rates. A power of n=1 for the bed concentration-bed shear stress relationship was to found give the best results. Similar results were found by Vinzon and Mehata (2003) for field data of the Amazon mouth in Brasil. The computed mud transport rates are shown in **Figure 5.13**. The magnitude of the peak values are quite good; the timing is less good which is caused by the application of a sinusoidal tidal velocity. The measured tidal velocity shows a pronounced asymmetry with time, see **Figure 5.13**. This latter effect cannot be represented by the TMUD-model.
The computed net tide-integrated mud transport is about 13000 kg/m/tide (37000 kg/m/tide for flood and 24000 kg/m/tide for ebb). The measured net tide-integrated mud transport is 8500 kg/m/tide
Figures 5.14 and **5.15** shows the computed mud concentrations at peak flood and ebb flow.

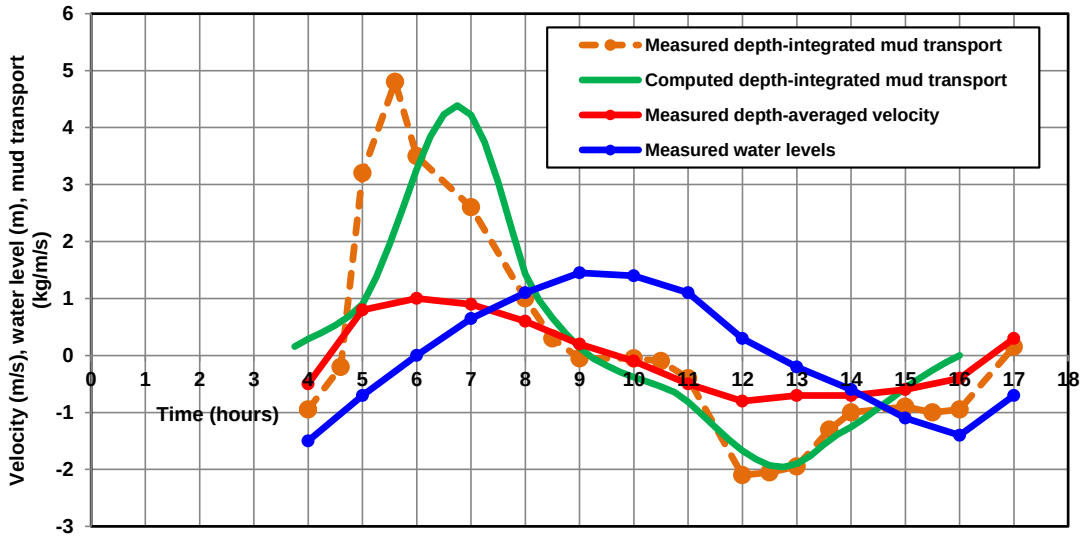

Figure 5.13 *Tidal variation of velocity, water levels, depth-integrated mud transport, location A, Ems river*

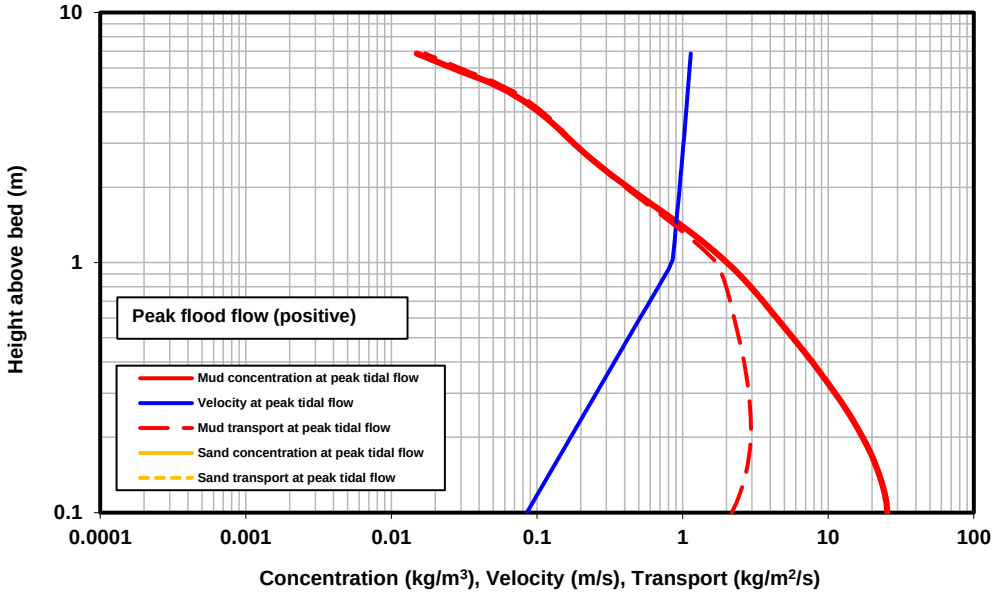

Figure 5.14 *Computed mud concentration profiles at peak flood flow at location A, Ems river*

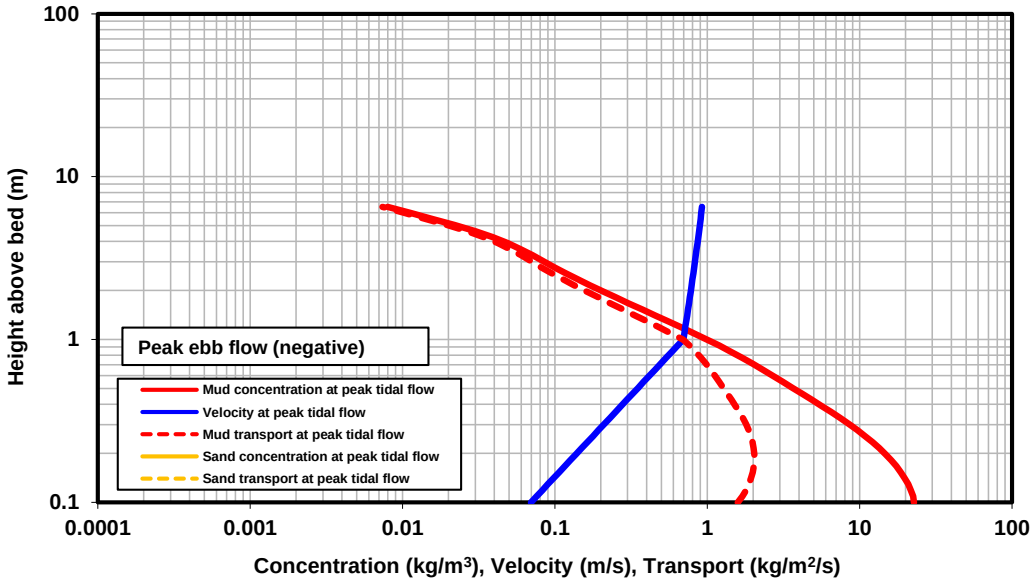

Figure 5.15 *Computed mud concentration profiles at peak ebb flow at location A, Ems river*

6. Time-dependent 2DV mud and sand transport model for tidal flow (SUSTIM2DV.xls)

6.1 General

The numerical SUSTIM-model solves the time dependent 3D advection-diffusion equation for suspended sediment concentrations. The 3D advection-diffusion equation can be solved when the following parameters are known: 1) flow field (u, v, w); 2) sediment mixing coefficients ($\varepsilon_{s,x}$, $\varepsilon_{s,y}$, $\varepsilon_{s,z}$); 3) settling velocity (w_s) and 4) sediment concentrations at all boundaries and at initial time. The 2DV-model is derived from the 3D-model by setting the lateral components to zero.
The sediment mixing coefficients are related to basic current and wave parameters. The settling velocity depends on the sediment concentration to include the effects of flocculation and hindered settling in mud suspensions.
The bed-boundary condition (reference concentration) is represented by an empirical equation specifying the near-bed concentration as function of the local bed-shear stress.
The velocities and mud concentrations are computed as a function of z and t; z=height above bed and t=time .
The grid points over the depth (25 to 100 points) are distributed according to an exponential function over the water column. The bed is defined at z=0. The grid points are distributed between z=0 and the water surface at each time.
The effect of the number of vertical grid points (NZ=10,25,50 and 100) on the computed sand concentration profile was studied for a channel with a constant depth of h=10 m and steady flow of 1.35 m/s (no tide). Other parameters are: sand d_{50}=0.2 mm; w_s=0.015 m/s, k_s=0.03 m z_a=0.05 m, β=1. The bed concentration for sand is set to 5 kg/m^3 (applied at z=0 m). The computed sand concentration profiles for NZ=10, 25, 50 and 100 are shown in **Figure 6.1**. The analytical Rouse concentration profile $c=c_a\ [((h-z)/z)(a/(h-a))]^{ws/(\beta\kappa u^*)}$ based on a parabolic mixing coefficient distribution is also shown. The computed values of the numerical SUSTIM2DV-model for NZ=50 and 100 are in good agreement with the analytical values in the lower half of the depth. The analytical concentrations are lower in the upper half due to parabolic mixing coefficient distribution, whereas a constant value is used in the numerical model. At least, 25 to 50 grid points are required for accurate results.
A detailed description of the SUSTIM2DV-model is given by Van Rijn (2023).

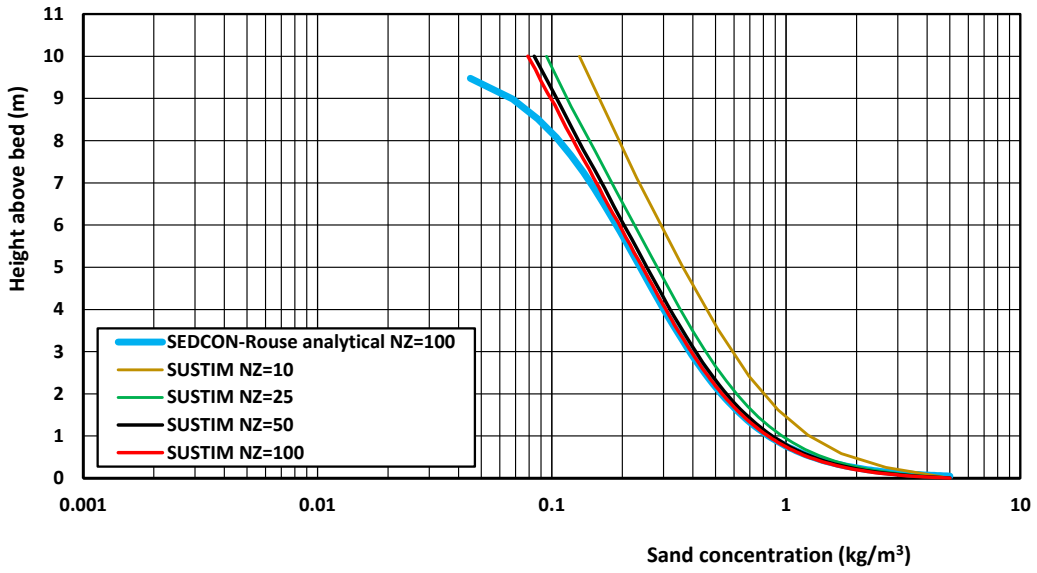

Figure 6.1 *Effect of vertical grid points on computed sediment concentration profile in steady current*

6.2 Flow field

The SUSTIM2DV-model can be used for conditions with a constant water depth or a varying water depth.

Tidal variation: $\eta_t=\eta_{max}\sin(\omega t)$ (6.1)

Water depth at boundary: $h_{o,t}=h_{MSL,o}+\eta_t$ (6.2a)

Current at boundary: $u_{o,t}=u_{mo}+u_{maxo}\sin(\omega t+\varphi)$ (6.2b)

Current along traject: $u_{x,t}=h_{o,t}\,u_{o,t}/h_{x,t}$ (6.3)

u_o= depth-averaged current velocity at x=0, u_{mo}= constant depth-averaged velocity at x=0 (input), u_{maxo}= depth-averaged amplitude of current velocity at x=0 (input), $h_{MSL,o}$= depth between bottom and mean sea level at x=0, η_{max}= tidal amplitude, h_o= water depth at inflow boundary (water depth outside channel), h_x= local water depth (bottom to surface), ω= $2\pi/T$; T= tidal period, x= longitudinal coordinate.
Equation (6.3) is used to determine the current velocity over a varying bed profile (pipeline trench, shipping channel, sediment mound). Additional equations are implemented in the model to represent oblique flow over a varying bed profile. Herein, only cases with flow normal to a trench, pit or channel are simulated.

The vertical distribution of the velocity at coordinate x is assumed to be logarithmic and is described as:

$u_{z,t}=(z/\delta_{fm})u_{b,t}$ for $z\leq\delta_{fm}$ (6.4a)

$u_{z,t}=u_t\,[(-1+\ln(h_x/z_o))]^{-1}\ln(z/z_o)]$ for $z>\delta_{fm}$ (6.4b)

$u_{b,t}=u_t\,[(-1+\ln(h_x/z_o))]^{-1}\ln(\delta_{fm}/z_o)]$ (6.4c)

with: $u_{b,t}$= near-bed velocity vector at level $z=\delta_{fm}$ at time t, u_t=depth-averaged current velocity
δ_{fm}= thickness of high-concentration fluid mud layer (input value), z= level above bed (m), h_x= water depth at time t, z_o= $0.033k_{s,c}$ = zero-velocity level [16], $k_{s,c}$ = current-related bed roughness (wave-current interaction is neglected).
The velocity inside the fluid mud layer (if present) is assumed to be linear, see Equation (6.4a).
The vertical fluid velocity (w) follows from the continuity equation for the fluid ($\partial u/\partial x+\partial w/\partial z=0$).

6.3 Basic sediment equations

The time dependent 3D advection-diffusion equation reads, as:

$$\partial c/\partial t+\partial(uc-\varepsilon_{s,x}\partial c/\partial x)/\partial x+\partial(vc-\varepsilon_{s,y}\partial c/\partial y)/\partial y+\partial((w-w_s)c-\varepsilon_{s,z}\partial c/\partial z)/\partial z=0 \quad (6.5)$$

with:
c= sediment concentration (volume), u, v, w= fluid velocities in x, y and z direction, w_s= settling velocity,
$\varepsilon_{s,x}$, $\varepsilon_{s,y}$, $\varepsilon_{s,z}$ = sediment mixing coefficients in x, y and z direction,
x= longitudinal coordinate, y= lateral coordinate (set to 1 m), z= vertical coordinate.
The 2DV advection-diffusion equation for uniform flow in longitudinal direction reads as:

$$\partial c/\partial t-\partial cw_s/\partial z-\partial(\varepsilon_s\partial c/\partial z)/\partial z=0 \quad (6.6)$$

with:
c= concentration (volume), w_s= settling velocity of suspended material, ε_s= sediment mixing coefficient.
In the case of a steady current ($\partial c/\partial t=0$; u=constant), Equation (6.6) gives the equilibrium concentration profile, as follows:

$$cw_s+\varepsilon_s dc/dz=0 \quad (6.7)$$

As the settling velocity and the sediment mixing coefficient are both dependent on the concentration, Equation (6.7) can only be solved numerically and is used at the inflow boundary. The sand and mud concentrations at initial time (t=0) are set to zero (c=0).
The bed-shear stresses at time t due to currents and waves are represented as:

$$\tau_{b,c}= \rho_w \kappa^2 u_b^2/[\ln(30z_b/k_{s,c})]^2 \quad (6.8a)$$
$$\tau_{b,c}= 0.125\ \rho_w \alpha_w f_c (u_c)^2 \quad (6.8b)$$
$$\tau_{b,w}= 0.25\ \rho_w f_w (U_w)^2 \quad (6.9)$$
$$\tau_{b,cw} =\tau_{b,c} + \tau_{b,w} \quad (6.10)$$

with: $\tau_{b,c}$=current-related bed-shear stress,$\tau_{b,w}$=wave-related bed-shear stress,
$\tau_{b,cw}$=bed-shear stress due to combined current and waves,
h=water depth, u_c= depth-averaged current velocity (m/s),
$U_w= (2\pi/T_p)A_w$=peak orbital velocity (linear wave theory),
A_w= peak orbital excursion, T_p= peak wave period,
$\alpha_w=[\ln(30\delta_b/k_a)/\ln(30\delta_b/k_{s,c})]^2\ [(-1+\ln(30h/k_{s,c}))/(-1+\ln(30h/k_a))]^2$= wave-related coefficient ($0<\alpha_w\leq 1$),
$f_w= \exp(-6+5.2(A_w/k_{s,w})^{-0.19})$= wave-related friction coefficient,
$f_c=0.24/(\log(12h/k_{s,c}))^2$= current-related friction coefficient,
h= water depth, δ_b=wave-related mixing layer near bed,
H_s= significant wave height, T_p= peak wave period,
$k_{s,c}$= current-related roughness, $k_{s,w}$= wave-related roughness,
k_a= apparent bed roughness for current (range 1 to 5 $k_{s,c}$),
ρ_s= sediment density (input value), ρ_w= fluid density (input value).

The effective bed-shear stresses at time t for sediment transport are represented as:

$$\tau_{b,c}^{/} = \mu_c\ \tau_{b,c} \quad (6.11)$$
$$\tau_{b,w}^{/} = \mu_w\ \tau_{b,w} \quad (6.12)$$

with: μ_c= current-related efficiency factor, μ_w= wave-related efficiency factor.

Sand: the reference concentration c_a is represented, as:

$$c_{a,sand}=0.015\ (1-p_{mud})\ (d_{50}/a)\ [(\tau_{b,cw}^{/}-\tau_{b,cr,o})/\tau_{b,cr,o}]^{1.5}\ (D_*)^{-0.3} \quad (6.13)$$

with: d_{50}= median particle diameter, $D_*= d_{50}[(s-1)g/\nu^2]^{0.333}$= dimensionless particle parameter,
$\tau_{b,cr}=(1+p_{mud})^2\tau_{b,cr,o}$= critical bed-shear stress of sand mixed with some mud,
$\tau_{b,cr,o}$= critical bed-shear stress of sand based on d_{50} (Shields' curve).
$\tau_{b,cw}^{/}= \mu_c\tau_{b,c}+\mu_w\tau_{b,w}$= effective bed-shear stress due to current and waves,
$\mu_c=f_c^{/}/f_c$= current-related efficiency factor,
$f_c= 0.24/[\log(12h/k_{s,c})]^2$= current-related friction coefficient,
$f_c^{/}=0.24/[\log(12h/(3d_{90}))]^2$=grain-related friction coefficient, d_{90}= grain size,
$\mu_w= 0.7/D_*$= wave-related efficiency factor ($\mu_{w,min}=0.14$, $\mu_{w,max}=0.35$ based on d_{50}),
$s=\rho_s/\rho_w$= relative density, ν= kinematic viscosity coefficient, ρ_s= sediment density (input value),
a= reference level above the bed, p_{mud}= fraction of mud (<0.062 mm) of top layer of bed.

Mud: the boundary condition at the bed is represented by the reference bed concentration $c_{a,mud}$, as follows:

$$c_{a,mud}=\alpha_{mud}[\tau_{b,cw}^{/}-\tau_{b,cr,e})/\tau_{b,cr,e}] \quad \text{for } du/dt>0 \text{ (accelerating tidal flow)} \quad (6.14a)$$
$$dc_{a,mud}/dz=0 \quad \text{for } du/dt< 0 \text{ (decelerating tidal flow; } c_{a,t}<c_{a+1,\ t-\Delta t}) \quad (6.14b)$$

with:
α_{mud}= erosion coefficient (input value), p_{mud}=fraction of mud of top layer of bed (input value),
$\tau_{b,cr,e}$= critical bed-shear stress for erosion (input value),
$\tau_b' = \mu_c\tau_{b,c}+\mu_w\tau_{b,w}$= effective bed-shear stress due to current and waves,
$\mu_c=f_c'/f_c$= current-related efficiency factor=1 for mud, μ_w= wave-related efficiency factor =0.35 for mud.

Equation (6.14b) means no upward flux of mud from the bed into suspension during decelerating flow; sediment settles on the bed at rate $c_{a,mud}w_s$.

The settling velocity is described, as:
Sand: the settling velocity of sand is assumed to be constant.
Mud: the mud settling velocity is concentration-dependent and represented as:

$$w_{mud} = \exp[\alpha_1 \ln(c) + \alpha_2 - \alpha_3]; \quad \text{for flocculation range } c \le 0.0025 \qquad (6.15a)$$
$$\alpha_1 = 0.182 \ln(w_{mud,max}/w_{mud,min})$$
$$\alpha_2 = 2.09 \ln(w_{mud,max})$$
$$\alpha_3 = 1.09 \ln(w_{mud,min})$$
$$w_{mud} = w_{mud,max}(1-c)^4 \quad \text{for hindered settling range } c > 0.0025 \qquad (6.15b)$$

with:
$w_{mud,max}$= maximum settling velocity at c=0.0025 (input value),
$w_{mud,min}$=minimum settling velocity at c=0.00001 (input value).

The settling velocity at height z is determined by using the concentration values at t-Δt.
Equation (6.15) with $w_{mud,max}$=0.001 m/s and $w_{mud,min}$=0.0001 m/s, is shown in **Figure 6.2**.

Using a concentration-dependent settling velocity, the transport of mud < 32 μm can be represented by one single fraction.

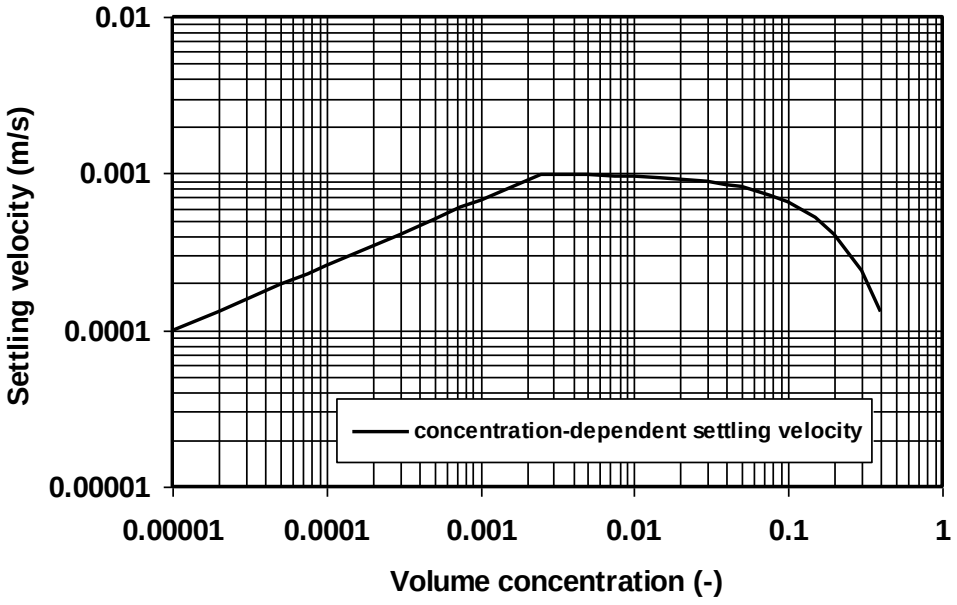

Figure 6.2 *Settling velocity as function of volume concentration; flocculation range for c<0.0025 and hindered settling range for c>0.0025; $w_{mud,max}$=0.001 m/s (1 mm/s), $w_{mud,min}$=0.0001 m/s (0.1 mm/s)*

For combined steady and oscillatory flow, the sediment mixing coefficient is modelled as:

$$\varepsilon_{s,cw} = [(\varepsilon_{s,c})^2 + (\varepsilon_{s,w})^2]^{0.5} \quad (6.16)$$

in which: $\varepsilon_{s,w}$= wave-related mixing coefficient (m²/s), $\varepsilon_{s,c}$= current-related mixing coefficient (m²/s).

Sand: the vertical distribution of the current-related mixing is parabolic-constant (**Figure 6.3**) over the depth:

$$\varepsilon_{s,c} = \varepsilon_{s,c,max} - \varepsilon_{s,c,max}(1-2z/h)^2 \quad \text{for } z/h < 0.5 \quad (6.17a)$$
$$\varepsilon_{s,c} = \varepsilon_{s,c,max} = 0.25\ \beta\ \kappa\ u_{*,c}\ h = 0.1\ \beta\ u_{*,c}\ h \quad \text{for } z/h \geq 0.5 \quad (6.17b)$$

with: β=ratio of sediment and fluid mixing coefficient (input parameter, default=1, range 0.5-1.5), κ=0.4=constant of Von Karmann, $u_{*,c}=(\tau_{b,c}/\rho_w)^{0.5}$=current-related bed-shear velocity, h=water depth.

The vertical distribution of the wave-related mixing is linear-constant (**Figure 6.3**) over the depth:

$$\varepsilon_{s,w} = \varepsilon_{s,w,bed} \quad \text{for } z \leq \delta_b \quad (6.18a)$$
$$\varepsilon_{s,w} = [\varepsilon_{s,w,bed} + (\varepsilon_{s,w,max} - \varepsilon_{s,w,b})\ (z-\delta_b)/(0.5h-\delta_b)] \quad \text{for } \delta_b < z < 0.5h \quad (6.18b)$$
$$\varepsilon_{s,w} = \varepsilon_{s,w,max} \quad \text{for } z \geq 0.5h \quad (6.18c)$$
$$\varepsilon_{s,w,bed} = 0.018\ \gamma_4\ \delta_b\ U_w \quad (6.18d)$$
$$\varepsilon_{s,w,max} = 0.035\ \gamma_3\ h\ H_s/T_p \quad \text{with } \varepsilon_{s,w,max} \leq 0.05\ m^2/s. \quad (6.18e)$$

with:
$\varepsilon_{s,w,bed}$= wave-related sediment mixing coefficient near the bed,
$\varepsilon_{s,w,max}$= maximum wave-related sediment mixing coefficient at mid-depth (z/h=0.5),
δ_b= wave-related mixing layer thickness near the bed, γ_3, γ_4= scaling calibration coefficients (range 0.25-1).

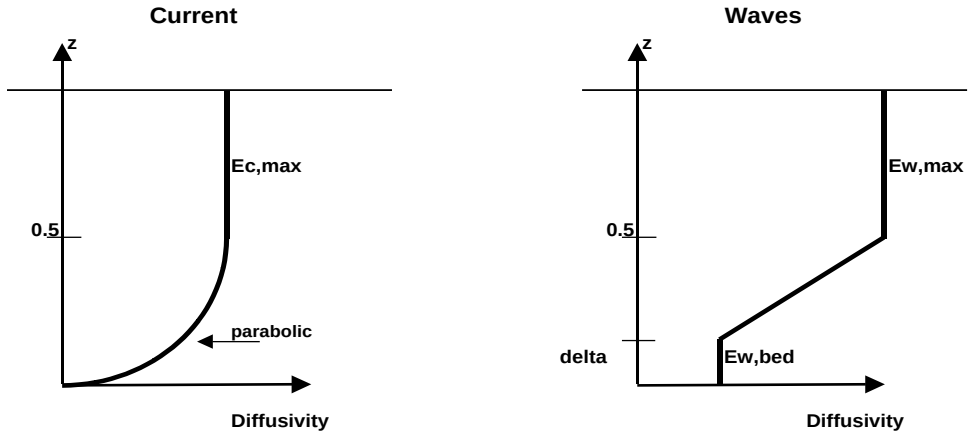

Figure 6.3 *Vertical distribution of mixing coefficients*

Mud: wave-related sediment mixing coefficient for muddy conditions is represented by by Equation (6.18); current-related sediment mixing coefficient distribution in the presence of fluid mud (if present) near the bed is represented by:

$$\varepsilon_s = \phi_d\ \varepsilon_{bfm} \quad \text{for } z \leq \delta_{fm} \quad (6.19a)$$
$$\varepsilon_s = \phi_d\ [\varepsilon_{b,fm} + (\varepsilon_{max} - \varepsilon_{bfm})\ (z-\delta_{fm})/(0.5h-\delta_{fm})]^n \quad \text{for } \delta_{fm} < z < 0.5h \quad (6.19b)$$
$$\varepsilon_s = \phi_d\ [(h-z)/(0.5h)]^n\ \varepsilon_{max} \quad \text{for } z \geq 0.5h \quad (6.19c)$$
$$\varepsilon_{max} = \gamma_1\ u_{*,c}\ h$$
$$\varepsilon_{bfm} = \gamma_2\ \varepsilon_{max}$$
$$\varepsilon_{min} = 0.001\ m^2/s$$

with:
δ_{fm} = thickness of fluid mud layer (input value), ε_{bfm}= sediment mixing coefficient in fluid mud layer, ε_{max}= maximum sediment mixing coefficient at mid-depth (z/h=0.5), ε_{min}= 0.001 m^2/s= minimum value at slack tide conditions, h= water depth, $u_{*,c}= (\tau_{b,c}/\rho_w)^{0.5}$= current-related bed-shear stress of current velocity vector, γ_1= scaling calibration coefficient (range=0.01-0.1; γ_1= 0.1 gives Equation 6.17b), γ_2= scaling calibration coefficient (range=0.05-0.5), n=exponent (input parameter; linear for n=1; approximately parabolic for n≅0.5), ϕ_d= turbulence damping coefficient (function of Richardson number), Ri= $[-(g/\rho)][d\rho/dz]/[(du/dz)^2]=[-(\rho_s-\rho_w)g/((\rho_w+(\rho_s-\rho_w)c)][dc/dz]/[(du/dz)^2]$ = Richardson number (salinity and temperature effects on the vertical density gradient are neglected), ρ= fluid-sediment mixture density=$\rho_s c+(1-c)\rho_w$, c= volume concentration.

The damping function is expressed as:

$$\phi_d=(1 + \alpha_d\, 2Ri^{0.5})^{-1} \qquad (6.20)$$

with: α_d= calibration coefficient (default=1; in range of 0 to 2), Ri=Richardson number (-).

Figure 6.4 shows the vertical distribution of the current-related mixing coefficient for mud with n=0.5, 1 and 2. The other parameters are: water depth is h=10 m; δ_{fm} = fluid mud layer = 1 m; ε_{max}= 0.05 m^2/s; ε_{bfm}= 0.01 m^2/s. For n=1, the mixing coefficient is linear between the fluid mud layer and the water surface; increasing from the top of the fluid mud layer up to mid-depth and decreasing from mid-depth to water surface. For n=0.5, the distribution is almost parabolic, as used for sand (Equation 6.17a) resulting in higher concentrations (lower concentrations for n=2).
Using a parabolic mixing coefficient distribution, the well-known Rouse-concentration profile is obtained.

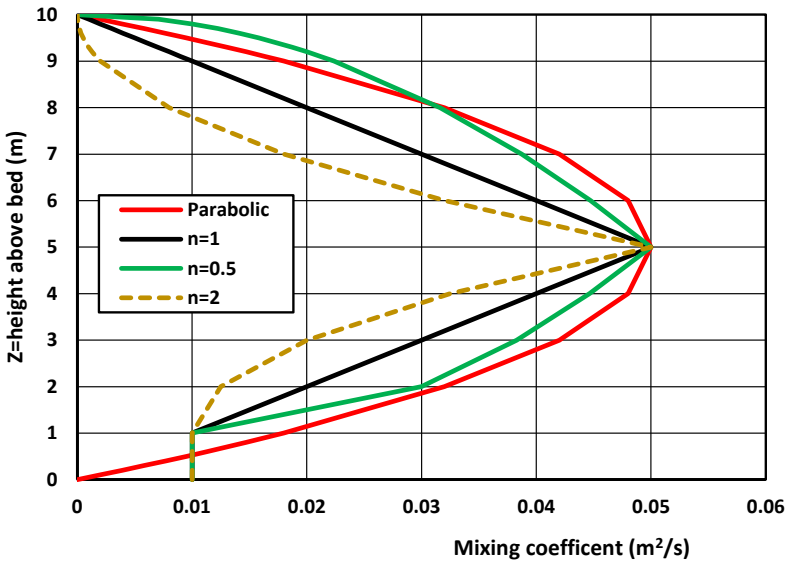

Figure 6.4 *Vertical distribution of current-related mixing coefficient for mud; water depth=10 m*

The depth-integrated sand or mud transport rate (kg/m/s) at each time t is computed as:

$$q_{s,sand,x}=\int_a^h (u_x c-\varepsilon_{s,x}\partial c/\partial x)\, dz; \qquad (6.21a)$$
$$q_{s,mud,x}=\int_a^h (u_x c-\varepsilon_{s,x}\partial c/\partial x)\, dz; \qquad (6.21b)$$

The bed load transport (kg/m/s) is computed as:

$$q_{b,sand,x}=0.5\ \gamma_b\ \rho_s\ d_{50}/D_*^{0.3}\ u'_{*c}\ [\tau'_{b,cw}-\tau_{b,cr}/\tau_{b,cr}] \quad (6.22)$$

with: γ_b=scaling coefficient, u'_{*c}=grain-friction-related bed-shear velocity due to current (m/s), $\tau'_{b,cw}$=effective bed-shear stress due to current and waves.

The bed load transport (kg/m/s) of mud is computed as:

$$q_{b,mud,x}= c_a\ a\ u_b \quad (6.23)$$

with: c_a= bed reference concentration (kg/m^3), a=reference level of bed concentration (m), u_b= near-bed velocity (m/s).

The bed level is computed from the sediment continuity equation (sources and sinks are neglected), as follows:

$$dz_b/dt + \gamma\ d(q_{b,x}+q_{s,x})/dx=0 \quad (6.24)$$

with; z_b=bed level (m) to a datum at location x and at time t; $q_{b,x}+q_{s,x}$=bed load transport plus suspended load transport (kg/m/s); $\gamma=1/\rho_{dry}$, ρ_{dry} =dry bulk density of bed (input value, kg/m^3).

6.4 Modelling of mud concentrations, transport and bed level changes

6.4.1 General

Results of various example cases and validation cases are shown. The validations cases refer to measured mud concentratios and mud transport in the the mouth of the Amazon river in Brasil and the Ems channel in Germany.

6.4.2 Effect of sediment mixing coefficient distribution

First, the effect of the sediment mixing coefficient distribution on the computed mud concentration profiles is explored by varying three coefficients of the mixing distribution: n=exponent=0.5 to 2, γ_1=gam1=0.01 to 0.05 and γ_2=gam2=0.001 to 0.005. The other input data are: water depth =10 m; no tide; steady current u=1 m/s; constant settling velocity w_s=0.0005 m/s (0.5 mm/s); critical bed-shear stress for erosion $\tau_{b,cr}$= 0.1 N/m^2; scaling coefficient bed reference concentration α_{mud}=0.000016; a=reference level= 0.05 m; no fluid mud; δ_{fm}=dfm=0.0001 m; bed roughness $k_{s,c}=k_{s,w}=k_a$=0.03 m; sediment density: ρ_s= 2650 kg/m^3, fluid density= 1025 kg/m^3, kinematic viscosity = 0.000001 m^2/s; timestep=4 s; NZ=50 grid points over water depth.
The effects of the n-coefficient (n=0.5, 1, 2) and the γ_1, γ_2-coefficients on the mud concentrations are shown in **Figure 6.5**. The bed concentration is constant (1 kg/m^3= 1000 mg/l) for all cases. The settling velocity is constant (w_s=0.5 mm/s) for all cases. The n-coefficient influences the vertical distribution of the sediment mixing coefficient; n=1 gives a linear distribution; n=2 gives a non-linear distribution with relatively low values in the lower and upper half of the water depth; n=0.5 gives a non-linear distribution with relatively high values in the lower and upper half of the water depth, which is close to the parabolic mixing coefficient corresponding to a logarithmic velocity profile. The γ_1 and γ_2-coefficients only influence the magnitude of the mixing coefficient at mid-depth and near the bed.
Using these three coefficients (n, γ_1, γ_2), a range of sediment concentration profiles can be represented from very uniform profiles for n=0.5, γ_1=0.5, γ_2=0.005 to very non-uniform profiles with a relatively low concentration at mid-depth (n=2, γ_1=0.01, γ_2=0.001). A lower n-coefficient gives higher concentrations in the water column. Lower γ_1 and γ_2-coefficients give lower concentrations in the water column. Default values are

n=1, γ_1=0.01 and γ_2=0.001 for the lower concentration range and n=2, γ_1=0.01 and γ_2=0.001 for the high concentration regime (fluid mud). When measured mud concentrations are available, the three coefficients can easily be calibrated.

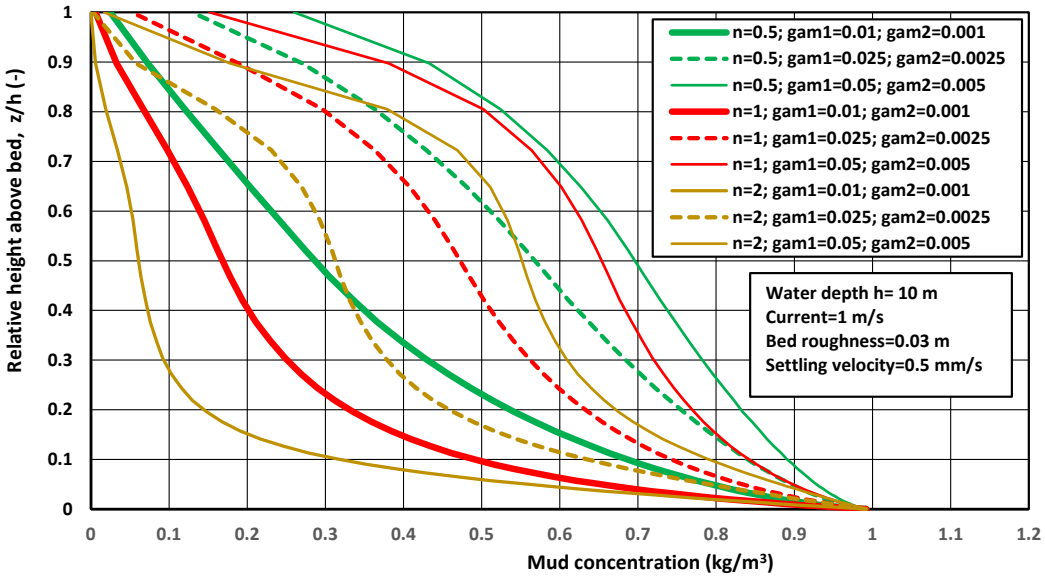

Figure 6.5 *Effect of coefficients n, gam1 (γ_1), gam2 (γ_2) on mud concentration*

Figure 6.6 shows measured mud concentrations during maximum flow conditions (around 3 to 4 hours before HW) in the tidal Holwerd ferry channel in the Dutch Wadden Sea. The peak tidal velocity is about 1 m/s. The water depth is about 4 m at peak tidal flow. The bed is composed of mud and silt in the range of 10-63 μm (settling velocity range 0.1 to 3 mm/s). The bed roughness is set to 0.01 m. Measured and computed mud concentrations are in very reasonable agreement for n=1.5; γ_1=0.025; γ_2=0.0035 and variable concentration-dependent settling velocity w_s=0.1-3 mm/s (mud-silt bed). Computed mud concentrations for a constant settling velocity (w_s=0.1, 0.5, 1 and 3 mm/s) are also shown. The mud concentrations are much too low in the upper part of the water column for w_s=3 mm/s. The mud concentrations are much more uniform over the depth for a settling velocity of 0.1 mm/s. Based on this, it is concluded that a variable concentration-dependent mud settling velocity is essential for a good representation of the measured mud concentrations, if a single fraction is used.

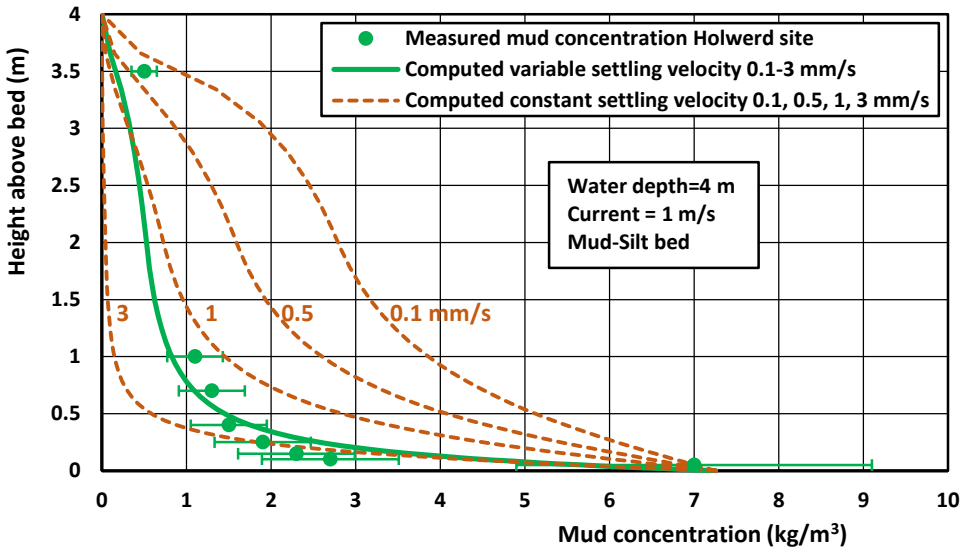

Figure 6.6 *Effect of settling velocitry on mud concentrations*

6.4.3 Mud concentrations and transport over tidal cycle

The SUSTIM2DV-model is used to compute the mud concentrations over two tidal cycles of 12 hours in a channel with depth of 10 m and a mud bed. The tidal amplitude is 1 m. The peak tidal current velocity of flood and ebb is 1.35 m/s. The mud settling velocity is constant at 0.5 mm/s. The critical bed-shear stress for erosion is 0.1 N/m^2. The bed roughness is 0.03 m. **Figure 6.7** shows the mud concentrations at 0.5, 1.5, 3, 5 and 8 m above the bed over the second tidal cycle based on 50 grid points over the depth.The depth-integrated mud transport and the depth-mean mud concentration defined as $q_{s,mud}/(u_{mean}\ h)$ are also shown. The following characteristics are given:

- the mud concentrations close to the bed (z<1 m) are maximum at the time of the maximum current velocity (t=3 and 9 hours); the maximum mud concentration close to the bed is about 6 kg/m^3 (bed-boundary condition); the maximum mud concentration at 0.5 m above the bed is about 4.2 kg/m^3;
- the concentrations at higher levels are maximum at approximately 1 hour (delay time) after the time of the maximum current and are minimum at approximately 1 to 2 hours after slack tide (current≅0 m/s);
- the concentrations around slack tide are still appreciable with values between 0.2 near the water surface and 1.5 kg/m^{3}near the bed; the mud concentrations at slack tide with low velocities (0 to 0.1 m/s over a period of about 1 hour in semi-diurnal tidal conditions) do not decrease to 0 kg/m^3, because the settling distance during this time period is about 3600x0.5=1800 mm=1.8 m which is much smaller than the water depth of 10 m;
- the variation range of the mud concentrations over the tidal cycle decreases at higher levels above the bed;
- the mud concentrations of the second tidal cycle after initial time (c=0 at t=0) are not fully representative for quasi-equilibrium conditions; more tidal cycles (spin-up time) are required to obtain a regular, repetitive cyclic behaviour of the mud concentrations.

Figure 6.8 shows the depth-integrated mud transport as function of depth-averaged current velocity during accelerating tidal flow and decelerating tidal flow. The mud transport is substantially higher during decelerating flow with particles settling towards the bed (hysteresis effect). The trend lines show that the mud transport can be represented by: $q_{mud,\ accelerating\ phase}= 9(u_{accelerating})^{1.1}$ and $q_{mud,decelerating\ phase}=15\ (u_{decelerating})^{1.3}$. This non-linearity effect is much weaker than that for sand ($q_{s,sand}\approx u^3$). These processes have also been observed at the Holwerd site in the Dutch Wadden Sea.

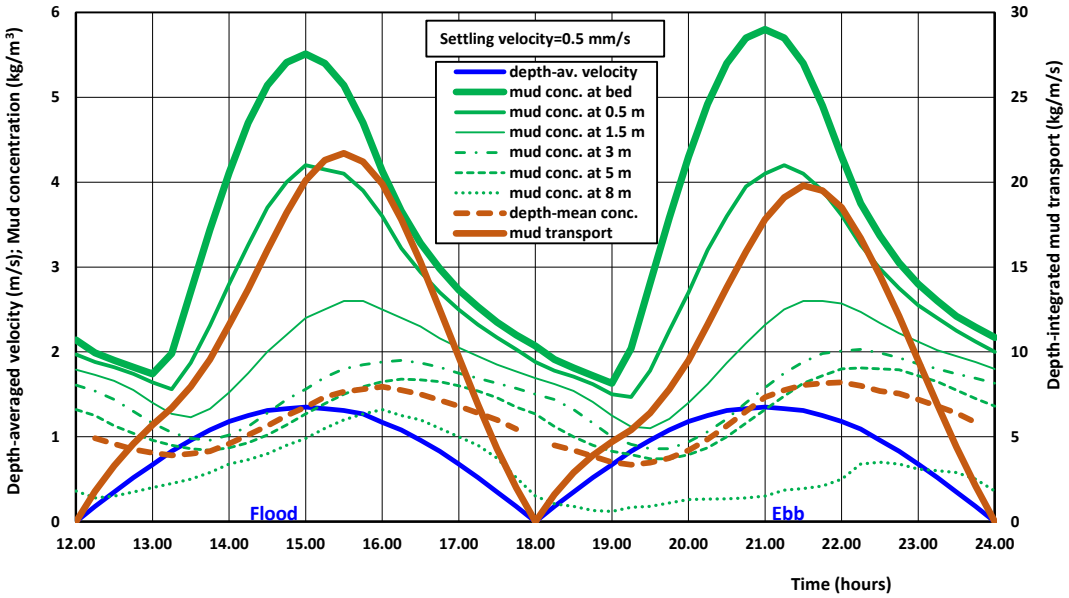

Figure 6.7 *Depth-averaged current velocity and mud concentrations at various levels above the bed over the second tidal cycle (50 grid points over the depth and output per 15 minutes)*

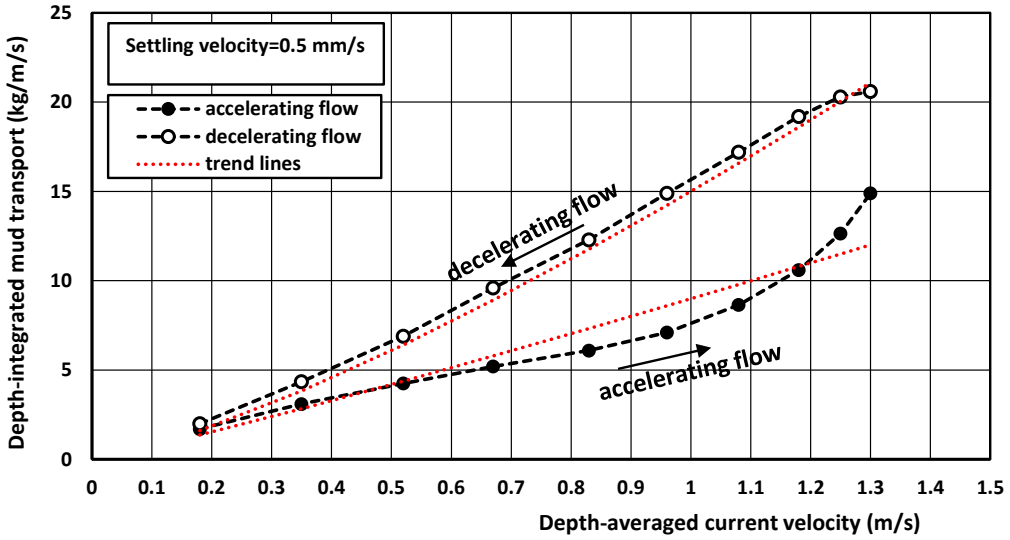

Figure 6.8 *Computed depth-integrated mud transport as function of depth-averaged current velocity*

6.4.4 Ems tidal channel

The model has been used for the simulation of the mud transport in the tidal Ems river in Germany. This tidal river is about 65 km from Hebrum weir to the mouth of the river at the large tidal Ems-Dollard bay. Upstream, near Hebrum, the width of the river measures about 60 m, increasing to about 120 m near Papenburg and around 600 m near the river mouth. The shallow and very muddy Dollard forms part of the Wadden Sea complex situated at the border between The Netherlands and Germany. The seabed of the estuary and the Ems river is (very) muddy. The data used herein refer to a location south of the city of Leer [31]. The measured depth-integrated mud transport rates are shown in **Figure 6.9**. The tidal range was about 2.8 m during the survey period. The salinity at location A was very small (<0.5 ppt). The peak flood velocity was about 1 m/s, the peak ebb velocity was about 0.8 m/s. The basic data are: water depth to mean level= 7 m, tidal amplitude=1.4 m; tidal period =12 hours; peak flood velocity=1 m/s; peak ebb velocity=0.8 m/s; maximum settling velocity=2 mm/s, minimum settling velocity=0.5 mm/s, bed roughness=0.01 m; ρ_s= 2650 kg/m^3, ρ_w= 1005 kg/m^3, ν= 0.000001 m^2/s, critical stress $\tau_{b,cr,mud}$= 0.1 N/m^2, α_{mud}= 0.0003, scaling coefficients mixing γ_1=0.05, γ_2=0.0025, n=2, α_d= 1 (Ri-approach for damping function), time step=4 s; NZ=50 grid points over depth.

The settling velocity was represented by a concentration-dependent settling velocity between $w_{mud,max}$= 0.002 m/s and $w_{mud,min}$=0.0005 m/s to represent the effects of flocculation and hindered settling. Turbulence damping was represented by a damping factor related to local Richardson number. The coefficient of the bed concentration was fitted (α_{mud}) to obtain the best agreement of computed and measured mud transport rates. The computed peak mud transport rates are shown in **Figure 6.9**. The magnitude of the peak values during flood and ebb are quite good; the timing during flood is less good. The measured peak mud transport during flood is about 30 minutes earlier than the peak current velocity, whereas the computed values show a delay time of about 0.7 hours.

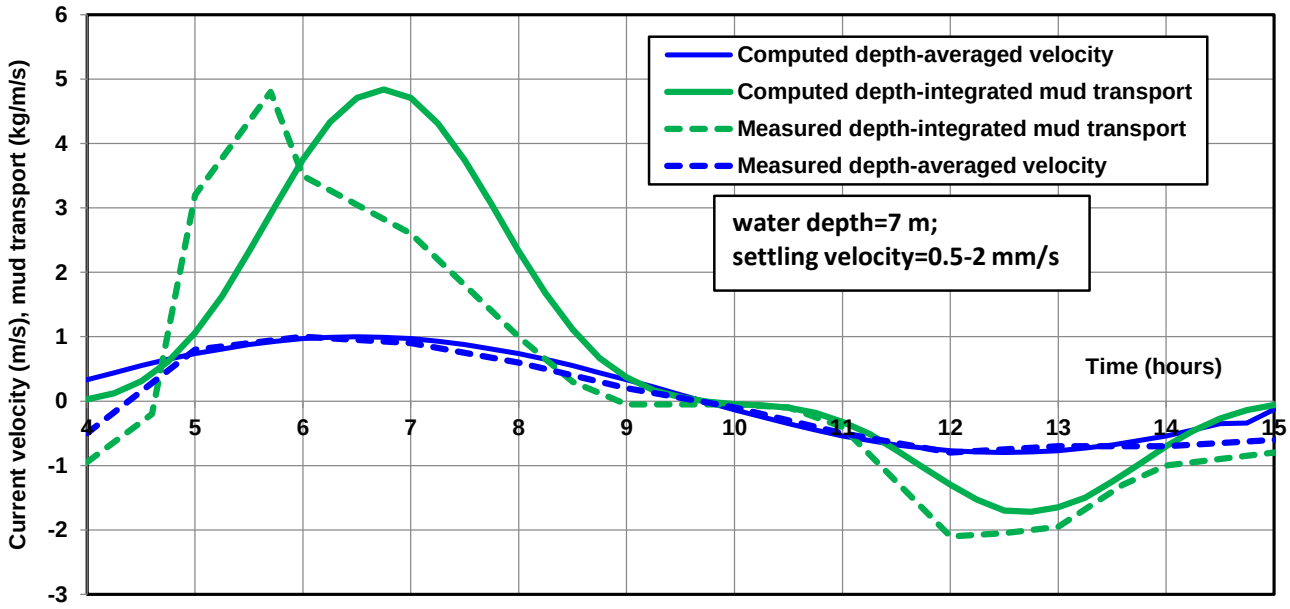

Figure 6.9 *Computed depth-integrated mud transport over tidal cycle, Ems river, Germany*

7. References

Bagnold, R.A., 1962. *Auto-suspension of transported sediment; turbidity currents, p. 315-319. Proc. Royal Society A, No. 1322, London, UK*

Bauamt fur Kustenschutz, Norden, 1987. *Tiefenstabilisierung von Aussentiefs mit Naturuntersuchungen am Nessmersieler Aussentief.*

Baugh, J.V. and Littlewood, M.A., 2006. *Development of a cohesive sediment transport model of the Thames estuary. Estuarine and coastal modeling, South-Carolina, USA*

BAW 2006/2007. *Anpassung der Fahrrinne von Unter- und Außenelbe an die Containerschifffahrt; Gutachten zur ausbaubedingten Änderung der morphodynamischen Prozesse, A3955 03 10062 H.1c*

De Nijs, M.A.J., 2012. *On sedimentation processes in a stratified estuarine system. Doctoral Thesis, Department of Civil Engineering, Technical University of Delft, The Netherlands*

Jiufa, L. et al., 2001. *Fluid mud transportation at water wedge in the Chiangjiang estuary, China. Sciences in China (Series B), Vl. 44*

Kineke, G.C. and Sternberg, R.W., 1995. *Distribution of fluid muds on the Amazon continental shelf, p. 193-233. Marine Geology, Vol. 125*

Kineke, G.C., et al., 1996. *Fluid-mud processes on the Amazon continental shelf, p. 667-696. Continental Shelf Research, Vol. 16, No. 5/6*

McAnally, W. et al., 2007. *Management of fluid mud in estuaries, bays and lakes. I: Present state of understanding on character and behavior. Journal of Hydraulic Engineering, ASCE, Vol. 133, No. 1, 9-22*

McAnally, W. et al., 2007. *Management of fluid mud in estuaries, bays and lakes. I: Measurement, modeling and management. Journal of Hydraulic Engineering, ASCE, Vol. 133, No. 1, 23-38*

Munk, W.H. and Anderson, E.R., 1948. *Notes on a theory of the thermocline. Journal of Marine Research, Vol. 3, 276-295*

Termes, 1990. *Sedimentation channels Rotterdam harbour (in Dutch). Report Q 1109, Delft Hydraulics, Delft*

Van den Berg, J.H. and Van Gelder, A., 1993. *Prediction of suspended bed material transport in flows over silt and very fine sand. Water Resources Research, Vol. 29, No. 5 p. 1393-1404*

Van Ledden, M. , 2003. *Sand-mud segregation in estuaries and tidal basins. Doctoral Thesis, Department of Civil Engineering, Delft University of Technology, Delft, The Netherlands*

Van Maren, D.S., Van Kessel, T., Cronin, K. and Sittoni, L., 2015. *The impact of channel deepening and dredging on estuarine sediment concentrations. Continental Shelf Research 95, 1-14*

Van Rijn, 1993. *Principles of sediment transport in rivers, estuaries and coastal seas.* *www.aquapublications.nl*

Van Rijn, L.C., 2011. *Principles of fluid flow and surface waves in rivers, estuaries and coastal seas.* *www.aquapublications.nl*

Van Rijn, L.C., 2015. *Principles of sedimentation and erosion engineering in rivers, estuaries and coastal seas.* *www.aquapublications.nl*

Van Rijn, L.C., 2016. *Review morphological effects of deepening of Elbe navigation channel, Germany. www.leovanrijn-sediment.com*

Vinzon, S.B. and Mehta, A.J., 2003. *Lutoclines in high concentration estuaries: some observations at the Mouth of the Amazon, p. 243-253. Journal of Coastal Research, Vol. 19, No. 2*

Voogt, L., Van Rijn, L.C. and Van den Berg, J.H., 1991. *Sediment transport of fine sands at high velocities. Journal of Hydraulic Engineering, ASCE, Vol. 117, No. 7.*

Winterwerp, J.C., 2001. *Stratification effects by cohesive and non cohesive sediment. Journal of Geophysical Research, Vol. 106, No C10, p. 22,559-22,574*

Winterwerp, J.C., 2006. *Stratification effects by fine suspended sediment at low, medium and very high concentrations. Journal of Geophysical Research, Vol. 111, C05012*

Winterwerp, J.C., 2011. *Fine sediment transport by tidal asymmetry in the high-concentrated Ems river: indications for a regime shift in response to channel deepening. Ocean Dynamics*

Xu, J., 1999a. *Grain-size characteristics of suspended sediment in the Yellow River, China. Catena, Vol. 38, p. 243-263*

Xu, J., 1999b. *Erosion caused by hyperconcentrated flow on the Loess Plateau of China. Catena, 36, 1-19*